PARAMETRIC ANALYSIS OF CONTINUOUS HIGH SHEAR WET GRANULATION

By

WEI MENG

A thesis submitted to the

Graduate School-New Brunswick

Rutgers, The State University of New Jersey

In partial fulfillment of the requirements

For the degree of

Master of Science

Graduate Program in Chemical & Biochemical Engineering

Written under the direction of

Fernando J. Muzzio, Ph.D

And approved by

_____

_____

_____

New Brunswick, New Jersey

JANUARY, 2015

ABSTRACT OF THE THESIS

PARAMETRIC ANALYSIS OF CONTINUOUS HIGH SHEAR WET GRANULATION

By WEI MENG

Thesis Director:

Fernando J. Muzzio, Ph.D

Wet granulation (WG) is widely used in the pharmaceutical industry. This technology has many advantages such as enhancing compression and powder handling, decreasing ingredient segregation and ensuring the content uniformity. Currently, a high level of interest exists in the continuous version of this technology, both by the US FDA, and by large pharmaceutical manufacturers. Continuous manufacturing can provide significant technical and business advantages relative to batch methods. They are more robust and controllable and can achieve the same production rates as batch processes in much smaller and thus less capital-intensive equipment. In recent years, different continuous WG techniques have been investigated. However, integration of these unit operations into a complete continuous tablet manufacturing line is still a bottleneck due to high production cost and poor understanding of the process. In this work, a continuous high-shear wet granulation process is examined based on a placebo formulation comprising of 69.7% ∂-lactose monohydrate, 29.3% microcrystalline cellulose and 1% Magnesium stearate. Two process variables (rotation speed, L/S ratio) and two design parameters (blade configuration and nozzle position) are selected for the I-optimal design. The collected granules are dried in a fluid bed drier to a desirable LOD (~ 3%). Granule

properties, such as particle size distribution (PSD), flow properties, density and compaction are characterized. The rotation speed and L/S ratio have the most significant effects on the granule properties. Mechanical dispersion regime controls the formation of granule nuclei in this case, resulting in broad particle size distribution and limited growth ratio.

ACKNOWLEDGEMENTS

This work was supported by National Science Foundation Engineering Research Center on Structured Organic Particulate Systems. I would not have been able to complete this work without the guidance and resources provided by my advisor Dr. Fernando J. Muzzio. He is always responsible and supportive; teach me a lot not only on academic research activities but also on many other aspects that I believe are very helpful in my future career. I also would like to thank my committee members: Professor Rohit Ramachandran and Professor Xue Liu for their time, carefully reviewing my work, and providing suggestions. I have had the pleasure to work with several graduate students whom I would like to acknowledge for teaching me particular methods and providing helpful advice: Yifan Wang, Sarang Oka, Sara Koynov, Pallavi Pawar, Bill Engisch, Juan Osorio, Abhishek Sahay. Further, I would like to acknowledge the Muzzio group for the wonderful friendship we built together during my graduate career.

I want to thank my parents for their unconditional support during my graduate research. Undoubtedly, I would not have been able to get this MS degree without the support of my fiancee Yingyue Zhang. Thank you.

Table of contents

ABSTRACT OF THE THESIS ii

ACKNOWLEDGEMENTS iv

Tablet of Contents v

List of tables viii

List of illustrations ix

Chapter 1 1

Introduction 1

1.1 Granulation Process Fundamentals 1

1.1.1 Wetting and Nucleation 3

1.1.2 Consolidation, Coalescence and Growth 6

1.1.3 Breakage and Attrition 9

1.2 Batch and Continuous Wet Granulation 9

1.3 Challenges and Outline of the Thesis 13

Chapter 2 15

Characterization of Continuous High Shear 15

2.1 Materials and Methods 15

2.1.1 Materials and Formulation 15

2.1.2 Design of Experiments 15

2.1.3 Manufacturing Process 16

2.1.4 Raw Materials Characterization 19

2.1.4.1 Particle Size Distribution 19

2.1.4.2 Penetration Time 20

2.1.5 Physical Characterization of Granules 23

2.1.5.1 Moisture Content 23
2.1.5.2 Particle Size Distribution 24
2.1.5.3 Hold up Measurement 24
2.1.5.4 Flow Properties 25
2.1.5.5 Density 26
2.1.5.6 Compaction 27
2.1.5.7 Particle Shape 27
2.2 Results and Discussion 27
2.2.1 Moisture Content 28
2.2.2 Particle Size Distribution 28
2.2.3 Hold up and Shear 35
2.2.4 Flow Properties 41
2.2.5 Density 44
2.2.6 Compaction 45
2.2.7 Particle Shape 51
Chapter 3 56
From Blends to Tablets: Influence of Formulation and Process Parameters 56
3.1 Objectives 56
3.2 Materials and Methods 56
3.3 Results and Discussion 58
3.3.1 Cohesion 58
3.3.2 Bulk Density 62
3.3.3 Tensile Strength 66
3.3.4 Correlation 70

3.4 Summary 71

Chapter 4 72

Conclusion and future Perspectives 72

4.1 Conclusion 72

4.2 Suggestion for future work 73

Reference 74

List of tables

Table 2-1. Materials and Formulation details……15

Table 2-2. Experimental Conditions……..15

Table 2-3 Particle size parameters of raw materials……..20

Table 2-4 I-optimal design and experimental results…….27

Table 2-5 Analysis of Variance for D50……31

Table 2-6 Analysis of Variance for % fines……...33

Table 2-7 Analysis of variance for Span……34

Table 2-8 Analysis of Variance for Hold-up…….37

Table 2-9 Analysis of Variance for Shear…….39

Table 2-10 Flow Properties of Selected Batches……...42

Table 2-11 Density of selected batches…….44

Table 2-12 Operation Conditions of Selected Batches……..45

Table 2-13 Tablets Data with the upper compression force of 10KN……...46

Table 2-14 Particle Size Distribution of Granules after Milling…… ..47

Table 2-15 Tablets Data for batch #4……48

Table 2-16 Tablets Data for batch #14……..49

Table 3-1. Pharmaceutical Powders with corresponding particle size……...56

Table 3-2. Values for the low(-1) and high(+1) levels of input variables investigated in the factorial design……...57

Table 3-3 Design of experiments followed by a 2^(4-1) fractional factorial design with two replicates…….58

List of illustrations

Fig. 1-1 Prototype of the continuous wet granulation line…….13

Fig. 2-1 Experimental set up……..18

Fig. 2-2 Blade Configuration with Forward and Backward Alternate……...19

Fig. 2-3 Particle size distribution of raw materials……20

Fig. 2-4 Syringe Penetration Test …….21

Fig. 2-5 The schematic (a) and the image (b) of the shear cell setup supplied with the FT3 Powder Rheometer (Freeman Technology, Inc.)……...25

Fig. 2-6 Particle Size Distribution of Granules before Milling…….29

Fig. 2-7 Contour Plot of D50 versus L/S Ratio and Rotation Speed…….31

Fig. 2-8 Contour Plot of % fines versus L/S Ratio and Rotation Speed……33

Fig. 2-9 Relationship between Span and L/S Ratio……...35

Fig. 2-9 Effects of L/S Ratio and Rotation Speed on Hold-up……..38

Fig. 2-11 Effects of Blade Configuration and Rotation Speed on Hold Up……..39

Fig. 2-12 Effects of L/S Ratio and Rotation Speed on Shear……40

Fig. 2-13 Effects of Blade Configuration and Rotation Speed on Shear……...41

Fig. 2-14 Flow Function and Yield Locus for the Selected Samples……43

Fig. 2-15 Flowability of Different Samples according to Jenike Classification of Bulk Flow Behaviour…….43

Fig. 2-16 Relationship between Hardness and D50……..48

Fig. 2-17 An illustration of compactability for #4……50

Fig. 2-18 An illustration of compactability for #14……...51

Fig. 2-19 Granules within the size range of 420-595 microns for selected batches……..53

Fig. 2-20 Correlation between eyecon camera and sieve analysis……54

Fig. 2-21 Granules under different size ranges……..55

Fig. 3-1 Pareto Chart of the standardized effects for cohesion……..58

Fig. 3-2 Main Effects Plot for cohesion…….59

Fig. 3-3 Interaction Plot for cohesion……60

Fig. 3-4 Cube Plot for cohesion…….61

Fig. 3-5 Optimization Plot for cohesion……62

Fig. 3-6 Pareto Chart of the standardized effects for bulk density……63

Fig. 3-7 Scatterplot of bulk density versus experimental order…….63

Fig. 3-8 Pareto Chart for bulk density after blocking and reducing model order……..64

Fig. 3-9 Main Effects Plot for Bulk Density……..64

Fig. 3-10 Interaction Plot for Bulk Density……...65

Fig. 3-11 Contour Plot for Bulk Density……...66

Fig. 3-12 Pareto Chart of the standardized effects for tensile strength…….67

Fig. 3-13 Main Effects Plot for Tensile Strength……..68

Fig. 3-14 Interaction Effects Plot for Tensile Strength…….68

Fig. 3-15 Cube Plot for tensile strength……69

Fig. 3-16 Residuals Plots for tensile strength……69

Fig. 3-17 Contour Plot between tensile strength, bulk density and cohesion……70

Chapter 1

Introduction

1.1 Granulation Process Fundamentals

Granulation is by definition any process of agglomerating small particles into larger, semi-permanent masses where the original particles can still be discriminated. [1] There have been various granulation techniques, including wet granulation, dry granulation and melt pelletization that have been widely utilized over the past decades across multiple industries such as the manufacturing of catalyst, food and agriculture product as well as pharmaceutical formulation and product manufacture. Specifically, in the pharmaceutical industry, the enlarged particle size typically ranges from 0.1 to 2.0 mm. The majority of granules are served as intermediate for compaction of tablets whilst others can be either packed as sachets or dispensed into capsules.[2]

Granulation is a popular processing method in the pharmaceutical industry due to its numerous advantages, such as enhancing powder flow properties and handling, [3-4] increasing content uniformity and compression characteristics of the drug, [5] decreasing dust and ingredient segregation, controlling the drug release rate, improving the appearance of tablets, etc. [6-7] Among granulation approaches, dry granulation is usually adopted for drugs that are sensitive to moisture and heat. Wet granulation is used for everything else due to its advantages, including dust elimination, single-pot processing and predictable granulation end-point. It improves powder performance by combining formulation composition and manufacturing process. The interaction between granulating

liquid and powder bed usually induces interparticle bonds, thereby modifying particle morphology and then resulting in different sizes of granules. [7-9]

Granulators with different operating principles have been employed in the pharmaceutical industry. High shear granulators are usually composed of a cylindrical or conical mixing bowl, a three-blade impeller and an auxiliary chopper, which can mix, densify and agglomerate the wetted particles by applying both the shear and compaction forces. [10] In batch fluid bed spray agglomeration, powders are fluidized and granulating liquid is sprayed onto the fluidized particles, which provides liquid bridges to agglomerate powders. Once desired granule size is achieved, spraying will terminate and then liquid will evaporate. It provides very low shear granulation and produces granules with high porosity and wide particle size distribution.[11] Besides, the process of wet extrusion, followed by spheronization, is used to produce numerous engineered, controlled release drugs containing high levels of API. The product characteristics for extrusion and spheronization usually include dense pellets, smooth coatable pellets, narrow particle size distribution and high yield and flowability. [12]

Continuous fluid bed granulators are widely utilized in the chemical, dairy and food industries and thus they have not been specifically designed and adopted for pharmaceutical production. They are usually horizontal moving bed granulators separated into distinct functional sections. They convey the dosed materials by vibrating the chamber or controlling the air flow. The produced granules are typically more porous than those generated by either high shear or extrusion granulation due to the relatively low shear and compressive forces. [13-14]

Twin screw extruder is the mostly investigated continuous granulation technique for pharmaceutical applications. The granulator is divided into different compartments serving as different roles during granulation like the long pitch transporting elements, short pitch transporting elements and kneading elements. [15]

All of these granulation processes are initiated by adding liquid and can be best described by several mechanism, mainly happening in three stages: 1) wetting, nucleation and binder distribution; 2) consolidation and coalescence and growth; 3) breakage and attrition, irrespective of the equipiments employed.

1.1.1 Wetting and Nucleation

Wetting and nucleation is the first phase of any wet granulation process involving the distribution of granulating liquid through the powder bed. [1] The contact of liquid binder with the powder surface can induce the formation of initial loose aggomerates. There are two extreme nucleation mechanisms that may take place during this process:

(1) droplet size is larger than that of a single particle. In this case, several consecutive stages are induced: a) the formation of droplets with different size distribution and varying frequency takes place at the spray nozzle; b) droplets impinged on powder bed surface and may possibly break into smaller droplet sizes; c) small binder droplets coalesce with each other to enhance the effective drop size when spray flux is very high or drop penetration time is long; d) the drops then spread across the powder surface and penerate into the bed due to the capillary effect and lead to the foregoing loose nuclei granule with a broad size distribution; e) mechanical mixing exerts shear force on large aggolomerates and break them into smaller entities.

All these stages are combined together to determine the granule size distribution when powders pass through spreay zone. The produced nuclei and granules usually possess porous structure with a lot of trapped air inside.

(2) primary particle size is larger than that of the binder droplet. The liquid droplets will deposit on the particle surface and coat the particles because of the collision between drop and particles. Typically, these small droplets will be sucked by capillary effects if the particles are porous, which induces the immersion nucleation. The resulting nuclei is usually saturated with liquid and gives rise to a relatively more compact granule structure. As a result, the wetting dynamics are essential in coating particle as well as the following growth stages. [1, 16]

Controlling the liquid drop size and liquid distribution is important for the wetting and nucleation processes. In some undesired cases, it can bring about a broad nuclei size distribution containing many fines, overwet granules, pastes and chunks, which can lead to subsequent ingredient segregation. Moreover, the mechanism of initial wetting and nucleation phase plays a pivotal role in the subsequent drying operations that generally seek to produce dried granules with moisture content less than 3%. Therefore, it is important to grasp the underlying mechanism and have a better control of granulation process. [17]

Based on the research of Hapgood et al. (2003),[16] the nuclei formation kinetics can be described by the penetration time, namely that the time that a droplet spends in completely penetrating into a porous powder bed surface. The penetration time depends on not only the powder hydrophobicity and fluid properties of viscosity and surface tension but also the consolidated condition of the powder bed-i.e., the effective pore size

of powder bed. For a specific formulation, Hapgood et al. (2002) [17] gave the formula to calculate penetration time t_p based on the measurable material properties:

$$t_p = 1.35 \frac{V_d^{2/3}}{\varepsilon_{eff}^2 R_{eff}} \frac{\mu}{\gamma_{lv} \cos\theta} , \qquad 1\text{-}1$$

where V_d is the drop volume; μ is the viscosity of liquid binder; θ is dynamic contact angle; ε_{eff} is the effective bed voidage for capillary driven flow; R_{eff} is the average micropore size; γ_{lv} is liquid surface tension.

Numerous assumptions are made when deriving this expression but the most essential one is that total voidage of the loosely packed powder bed is considered as uniform cylindrical pores. Practically, the liquid droplet may not have sufficient time to entirley penetrate into the powder and form a nucleus due to interference of mechanical shear forces or finite residence time in a continuous process.

A dimensionless group, called the dimensionless spray flux ψ_a is defined to characterize the spray zone in granulator, which takes into account the liquid flow rate, binder drop size and powder flux. In other words, it considers the competition between liquid spray rate and new powder exposure rate. A low spray flux means that the nozzle produce more fine or well dipersed droplet, which is conducive to minimizing the drop overlap and enhances granulation performance. When introducing the liquid binder by dripping mode, ψ_a is still useful; in this scenario the spray area is considered to be equivalent to the cross-sectional area of the liquid column. Lister et al. (2001) [18] gives the expression of dimensionless spray flux as

$$\Psi_a = \frac{3\dot{V}}{2\dot{A}d_d} \qquad 1\text{-}2$$

where $\dot{V}$ is the volumetric spray rate; $\dot{A}$ is the area of spray zone that powder flux through; d_d is droplet diameter.

As previously introduced, wetting and nucleation can be dominated by different mechanisms, depending on formulation properties and operation parameters. By combining the drop penetration time, which describes single drop behavior determined by material properties, with the spray flux describing multiple drop interactions, which is controlled by operation variables Hapgood et al. (2003) [16] proposed the nucleation regime map. The ordinate is defined as the dimensionless drop penetration time τ_p,

$$\tau_p = \frac{t_p}{t_c} \qquad 1\text{-}3$$

where t_c is the circulation time for a packet of powder to return to the spray zone.

Ideally, one droplet should produce one nucleus. The drop controlled nucleation occurs when both τ_p and ψ_a are less than 0.1, namely that droplets are well dispersed and that drops penetrate fast enough to avoid contacting another partially absorbed drop on the powder bed. In the mechanical dispersion regime, mechanical mixing and agitation dominate the nucleation process and the drop coalescence occurs giving rise to many fines and lumps at low shear force condition. Finally, in the intermediate region, the granulation process is very sensitive to the variations in nucleation zone.

1.1.2 Consolidation, Coalescence and Growth

The wetting and nucleation stage may result in two possible forms of particles, which will be further converted during the subsequent consolidation and growth stages. If the particle size is larger than that of the binder droplet, particles will leave the spray zone with a layer of liquid binder coating them, otherwise loosely packed and satuated nuclei granules will be created. The subsequent consolidation with neighbouring particles can densify the granules while coalescence may lead to the granule size enlargement.

Net granule growth depends on the balance between granule kinetic energy before collision and the corresponding energy dissipated during the collision. Specifically, in terms of deformable granules, mechanical energy will be dissipated via plastic deformation and friction at the surface of wetted granules due to the relatively high material viscosity. [19]

In pharmaceutical granulation, the growth behavior is determined by both granule deformation induced by collision and moisture content of granules. Therefore, the two dimensionless groups, Stokes deformation number and maximum granule pore saturation, are utilized to map the granulation behavior. The deformation number St_{def} was first proporsed by Tardos et al. (1997) [20] and later adopted by Iveson et al. (1998) [19].

$$St_{def} = \frac{\rho_G U_c^2}{2Y} \qquad 1\text{-}4$$

where ρ_G is the granule's density, U_c is the relative collision velocity and Y is the dynamic yield strength of granules. With respect to liquid saturation, maximum pore saturation is used because the saturation extent varies with compaction.

$$s_{\max} = \frac{w\rho_s(1-\varepsilon_{\min})}{\rho_l \varepsilon_{\min}} \qquad 1\text{-}5$$

where w is the mass ratio of liquid to dry powders, ρ_s is the true density of particles, $\varepsilon_{\min}$ is the minimum porosity, which is a complex function of specific formulation properties, liquid content and operation parameters, ρ_l is the liquid density.

One major assumption is that liquid spraying has been well controlled and thus achieved good distribution-i.e., the operation condition is within the drop-controlled region in terms of wetting and nucleation stage. When the maximum pore saturation is low, there is no enough liquid to achieve the granule coalescence and nuclei will only form nuclei due to Van de Waals forces that may break at the initial wetting-nucleation stage. Particles will not growth further but remain as dry-free flowing powders.

When the $\varepsilon_{\min}$ is at the intermediate level, granules will grow steadily, provided that they are deformable and consolidate very soon, otherwise the induction growth will take place as the yield strength of granules is large compared with the impact kinetic energy.

Induction growth is related to low material exchange rate in which period little granule growth happens. As a result, the addition of more liquid is necessary to promote granule growth. If the liquid content is very high ($\varepsilon_{\min}$ >1), granules will tend to get over-wetted and become a slurry. Moreover, steady growth is desirable because the granulation process are more robust to raw material properties and process operation conditions, which can be achieved with a St_{def} from 0.001 to 0.2. The granules in steady growth usually contact with each other in a large area during collision and can induce the coalescence under relatively low liquid saturation level. Finally, if St_{def} is larger than 0.2, the undesirable crumb behavior will occur, which produces granules that are too fragile to

withstand the shear forces present in the granulator. Consequently, granules will stop growing. [19, 21-23]

1.1.3 Breakage and Attrition

In this final mechanism, two phenomena will happen simultaneously-i.e, breakage of wet granules in the granulator and fracture of dried granules in the granulator or subsequent unit operations such as fluidized bed dryer and blender. Compared with the first two mechanisms, there have been relatively less investigation on breakage and attrition, but it is important to consider these phenomena as they may impinge on the granule properties, especially the size distribution. For example, in high shear granulators, the friction between blades or granulator wall with granules can produce substantial amounts of dusty fines, thereby decreasing the mean particle size and broadening the particle size distribution. As the purpose of granulation is to increase particle size, uncontrolled breakage can lead to process failure. [23-24]

To predict the threshold of wet granule breakage, Tardos et al. (1997) [20] considered the Stokes deformation number. They proposed that when St_{def} is larger than a specific value-i.e., when applied kinetic energy during collision exceeds the required energy to break, then granule breakage occurs, which is labeled as a boundary in the growth regime map of St_{def} =0.2. Therefore, it is essential to control granule turnover or the tip speed of the granulator to avoid excessive breakage and attrition.

1.2 Batch and Continuous Wet Granulation

Based on the definition of US FDA, [25] a batch process utilizes “a specific quantity of a drug or other material that is intended to have uniform character and quality, within

specified limits, and is produced according to a single manufacturing order during the same cycle of manufacture". In general, the product quality is assessed by off-line analytical tools when the predictable endpoint is reached. If it fails to satisfy the predefined quality parameters, the whole batch of materials must be discarded or reprocessed. Continuous manufacturing, in contrast, is in accordance with the principle of "one in, one out" by continuously adding raw materials to the process and simultaneously collecting products at the end of the manufacturing line. [26]

Unlike some other industries, such as food, polymer, dairy and electronics, the pharmaceutical industry has been reluctant to adopt continuous process for several reasons. For instance, continuous manufacturing technologies are especially suitable for large volume production that often exceeds the demand in the pharmaceutical industry. In addition, the high profit margins and concerns regarding regulatory approval have retarded the implementation of continuous processes.[27] This situation has changed dramatically in the last five years. A high level of interest exists now in continuous technology, both by the US FDA, and by large pharmaceutical manufacturers driven by the superior controllability of continuous processes. Continuous manufacturing methods can provide significant technical and business advantages relative to batch methods. As has been demonstrated in other process industries, continuous manufacturing methods are more robust and controllable, which enhances product uniformity, decreases the amount of materials failing to satisfy the quality parameters and improves production efficiency. They also achieve the same production rates as batch processes in much smaller and thus less capital-intensive equipment. Moreover, the scale-up challenges can be overcome by

running the operation for a longer time instead of changing to a larger capacity equipment.[27-28]

In addition, the US FDA has increasingly emphasized the application of Quality by Design[29-32] and Process Analytical Technology (PAT) methods in pharmaceutical manufacturing[33], thus promoting the adoption of continuous process, which is particularly suitable for real-time monitoring and automation.

In recent years, several continuous wet granulation techniques have been developed. [27] Most commercialized continuous fluid bed granulators are adopted in the chemical and food industries. In these systems, raw materials are dosed continuously at the inlet zone and conveyed horizontally to the following different functional sections, such as mixing, spraying, drying and cooling, because of air flow from distributor plates, vibration of processing chamber, or auger conveyors.[14, 34-37] Recently, Glatt developed the GPCG2 LabSystem, which is a continuous fluid bed granulator/drier designed for development and manufacturing of solid materials.

Another continuous wet granulation technique for pharmaceutical applications that has been examined in the literature is the extrusion with twin-screws rotating inside a barrel. This method comprises of multiple components, such as conveying elements, mixer elements and kneading blocks, to continuously transport, mix and agglomerate wetted powders driven by the energy from shear force or densification. [15, 27, 40] Using extruders as continuous granulators for pharmaceutical applications was first introduced by Gamlen et al. (1986) [38] and Lindberg et al. (1987) [28, 39]

Currently, the majority of studies focus on characterizing granulation performance with different process or design parameters as well as formulation properties. Djuric et al.

(2010) investigated the agglomeration behavior of a twin-screw extruder with varying material throughput and concluded that throughput had a large effect on granules particle size distribution.[41] EI Hagrasy et al. (2013) validated the robustness of a twin screw granulator under different formulation properties, liquid to solid (L/S) ratio and binder distribution method.[42] Djuric et al. (2008) and Thompson et al. (2009) investigated the impact of screw configuration on the granulation of lactose monohydrate. They indicated that desirable granule properties, such as particle size distribution and porosity, as well as tablet properties such as tensile strength can be achieved through a suitable selection of conveying elements, kneading and combing mixer elements.[43-44] Dhenge et al. (2010) and Vercruysse et al. (2012) investigated the influence of process variables such as powder feed rate, screw speed and L/S ratio, together with viscosity of granulation liquid, on granules residence time distribution and physical properties.[45-46] Lee et al. (2013) and Keleb et al. (2002) compared the performance of twin screw granulator and conventional high shear granulator by characterizing granules properties and revealed that twin screw granulator had a distinct granulation mechanism and might be a more suitable alternative for high shear granulation in pharmaceutical industry. [40, 47]

Vervaet et al. (2005) reviewed the development of continuous granulation in pharmaceutical industry and introduced some other techniques such as spray-drying, roller compaction, instant aggomerators, etc. Some of these techniques are specifically designed for pharmaceutical purposes while others could be introduced in the pharmaceutical field with some minor modifications. [27]

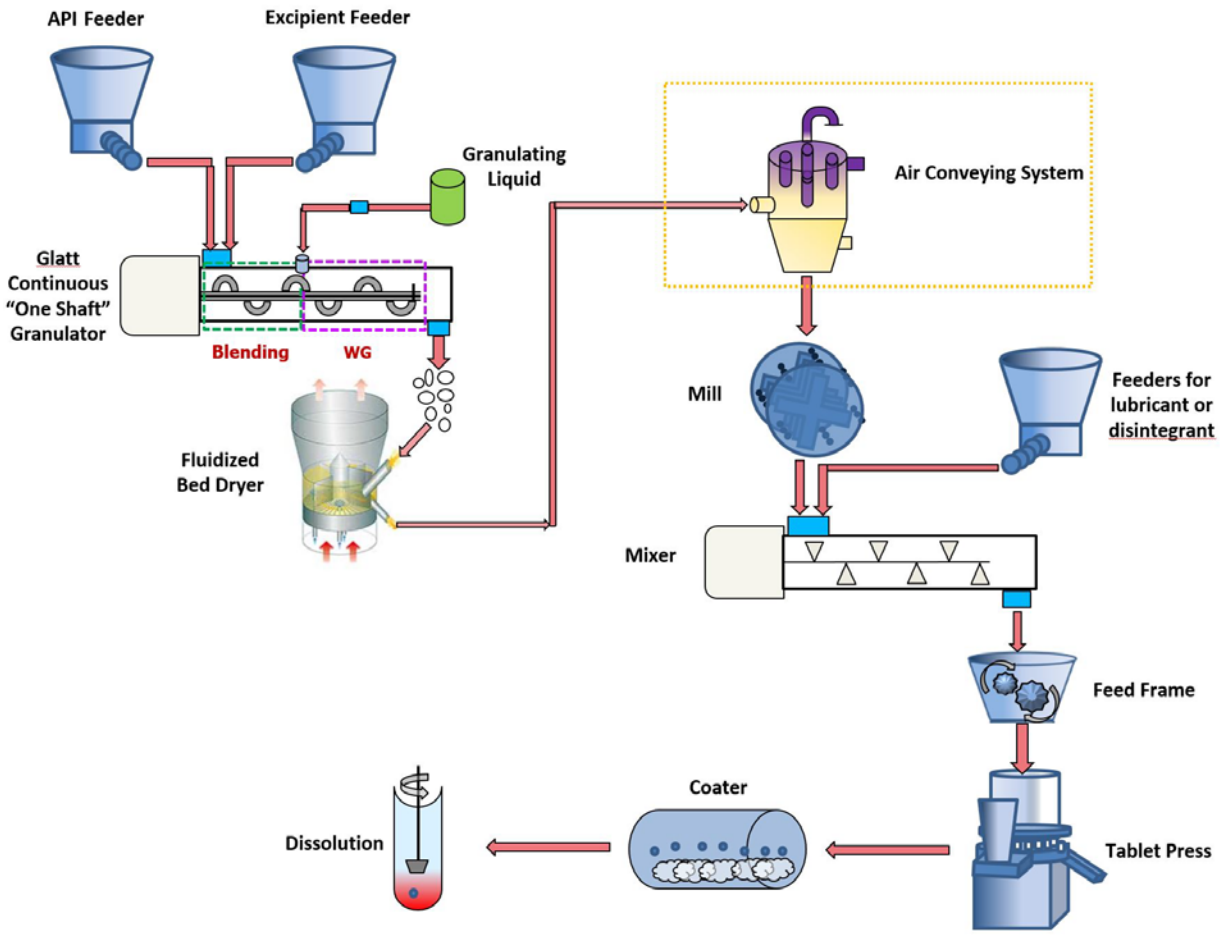

Fig. 1-1. Prototype of the continuous wet granulation line

1.3 Challenges and Outline of the Thesis

Despite the research on different continuous wet granulation techniques, incorporating this unit operations into a complete continuous tablet manufacturing line, namely from individual powder components to the coating of tablets, is still a bottleneck. It is partly due to the need to achieve desirable granule properties and the complexity of the process, which typically involves twice as many steps and components as direct compression.

However, the continuous high-shear mixer granulator, shown in Figure 1-1, can enable a fully continuous tablet manufacturing line. Also, successful implementation of such a system will enhance the mechanistic understanding of wet granulation in continuous

systems by enabling the investigation of effects of process variables, design parameters and formulation attributes on granule characteristics. Finally, experimental results obtained in this system can be utilized for the development and validation of models and process optimization and control.

This thesis focuses on characterizing a commercialized continuous high shear granulator from Glatt. It is organized as follows. Materials, methods and experimental conditions are presented in section 2.1. Results and discussion of granule physical properties are presented in section 2.2. Conclusions and future work are presented in Chapter 4.

Chapter 2

Characterization of Continuous High Shear Wet Granulation

2.1 Materials and Methods

2.1.1 Materials and Formulation

The placebo formulation studied here consists of a 7:3 mass ratio of α-lactose monohydrate 200M to microcrystalline cellulose (Avicel® PH101) . The quantitative compositions and supplier of each material are shown in Table 2-1. Intragranular components were used to manufacture granules while magnesium stearate then was mixed with milled granules to make tablets.

Table 2-1. Materials and Formulation details

Ingredient	%w/w	vendor
Intragranular components		
α-lactose monohydrate 200M	69.3	Foremost Farms USA
Microcrystalline cellulose (Avicel PH101)	29.7	FMC Biopolymer
Extragranular component		
Magnesium stearate	1	Mallinckrodt

2.1.2 Design of Experiments

Table 2-2. Experimental Conditions

Process Parameters	
Flow Rate (kg/hr)	10
Rotation rate (RPM)	133, 275, 415, 538, 660
L/S Ratio	0.1, 0.2, 0.3
Granulator Design Parameters	
Blade configuration name: blade direction, Blade angle (angle with the shaft)	1. F/S-Alternate blades directing in forward and straight, blade angle-45°/90° 2. F/B-Alternate blades directing in forward and Backward, blade angle-45°

Nozzle Positions	Position 1 (above the 12th blade from granulator inlet, 24 blades in total) Position 2 (above the 8th blade from granulator inlet, 24 blades in total)
Formulation	
Feeder 1- ∂-lactose monohydrate (Regular)	7 kg/hr
Feeder 2- microcrystalline cellulose (Avicel PH101)	3 kg/hr

Note that the levels of these two quantitative variables and two categorical variables, rotation speed (5 levels), L/S ratio (3 levels), blade configuration (2 levels) and nozzle position (2 levels), form an irregular experimental region-i.e., not a cube or a sphere. Therefore, standard designs may not be the best choice. In addition, D-Optimal designs are most appropriate for screening experiments because the optimality criterion focuses on precise estimates of the coefficients. In contrast, I-Optimal designs minimize the average prediction variance inside the region of the factors, which makes it more appropriate for prediction. Thus in this study an I-optimal design generated by the JMP® software from SAS was used as the experimental design. The total flow rate of dry powders was fixed at 10 kg/hr because of the processing ability of the following unit operation, fluidized bed dryer. Two process variables and two design parameters are selected for the I-optimal design, namely five levels rotation speed (133RPM, 275RPM, 415RPM, 538RPM and 660RPM), three levels L/S ratio (0.1, 0.2 and 0.3), two levels blade configuration (forward/backward and forward/straight) and two levels nozzle position (P1 and P2). A total of 38 batches were manufactured for this DoE.

2.1.3 Manufacturing Process

The K-Tron KT35 twin screw loss-in-weight feeder is used for dosing α-lactose monohydrate 200M while K-Tron KT20 is for microcrystalline cellulose. All the experiments were conducted in the continuous high shear granulator from Glatt as shown in Fig 2-1. There are three different types of blades including 60°, 90° and 120° mounted on horizontal shaft. As powders are fed into the granulator, the shaft along which three types of blades are mounted pushes the dry powders forward and promotes both dispersive axial mixing and convective cross-sectional mixing. The granulation process commences immediately once the mixtures reach the location where the nozzle is positioned and where granulating liquid (water) is fed via a pump. Powder mixing coupled with different granule formation mechanisms, (i.e. nucleation, coalescence, consolidation and attrition or breakage), continue along the axis of blender the outlet of the granulator is reached. The blade configuration for the first nozzle position with forward and backward alternate is shown in Fig 2-2. Similarly, substituting the straight blades for curved ones can generate another configuration. The first five blades under both dry powder feeding port and granulating liquid feeding port are setting as forward pushing blades to prevent powders from blocking the granulator. For all the experiments, water was introduced onto the powder bed only by dripping mode.

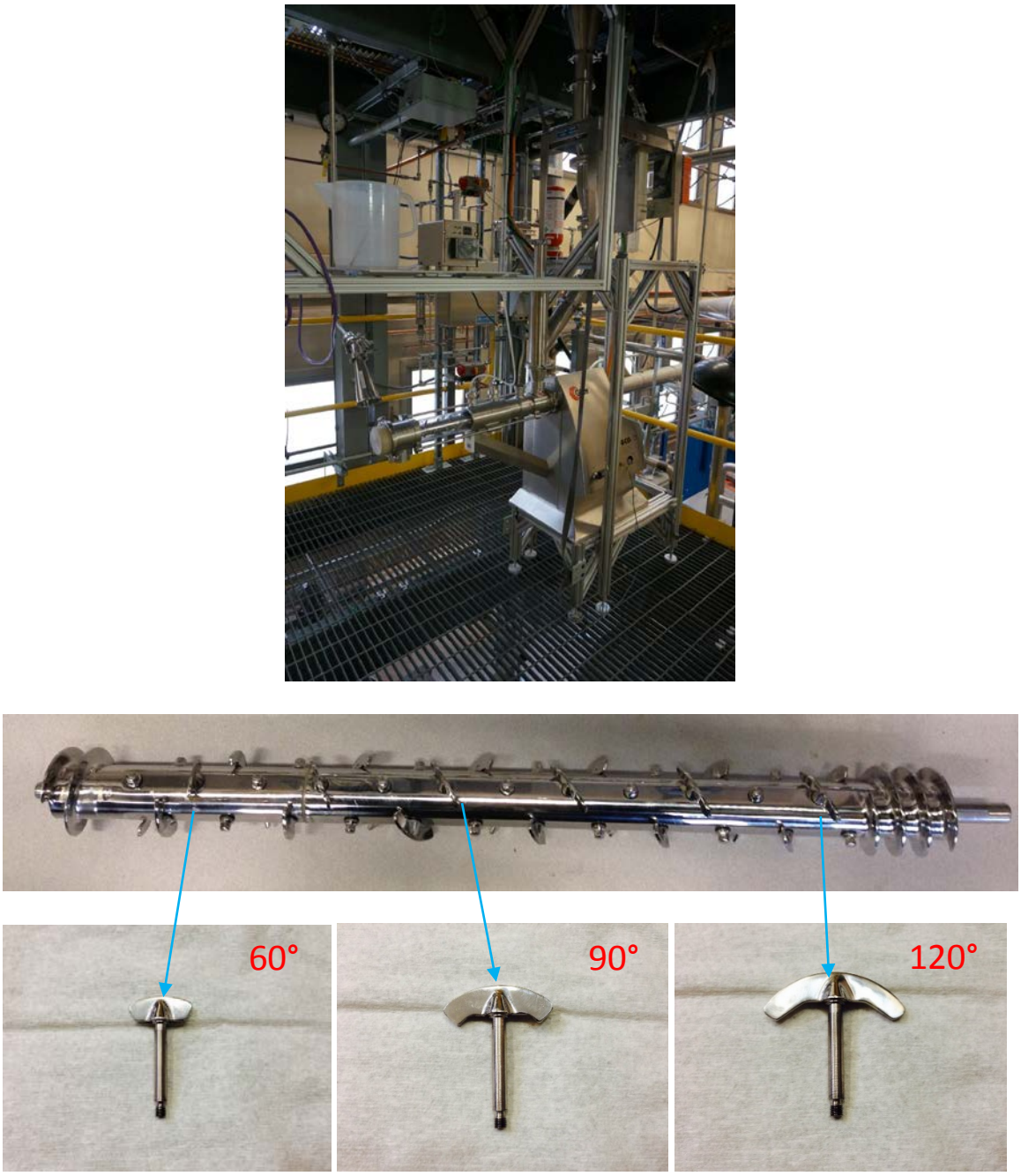

Fig. 2-1 Experimental set up

(a) ⇩ Powder inlet ⇩ Nozzle Position

Blade #	1	2	3	4	5	6	7	8	9	10	11	12	13	14	15	16	17	18	19	20	21	22	23	24
Blade Direction	\	\	\	\	\	/	\	\	/	\	/	\	/	\	/	\	/	\	/	\	/	\	/	\
Blade Type	60	90	60	90	60	90	60	90	120	90	60	90	90	90	90	90	90	90	90	120	60	120	60	120

*/ conveying; \ reverse conveying; | no conveying effect

⇩ Powder outlet

Fig. 2-2 Blade Configuration with Forward and Backward Alternate

The overall powder feeding rate was kept constant at 10 kg/hr for all batches. The collected granules passed through a 5-mesh screen to remove lumps and then dried in the fluid bed drier at 50℃ to a desirable loss on drying value less than 3.0%. The dried samples were then evenly spread on a large aluminum foil pans on which 9 sampling points were selected to obtain representative granules for particle size distribution test. Then 8 batches with D50 larger than 120 microns were selected for further characterization. These samples were passed through a Quadro Comil running at 2300rpm using a 045R of 1.1mm opening screen, which was able to provide sufficient de-lumping effciency. The 1% Magnesium Stearate was then mixed with milled materials in LabRAM mixer from Resodyn Acoustic Mixers for the following characterization like flow properties, density and compaction. The data generated from this I-optimal design were analyzed by JMP® statistical software.

2.1.4 Raw Material Characterization

2.1.4.1 Particle Size Distribution

The particle size of α-lactose monohydrate 200M, Avicel PH101 and the dry mixture of 69% lactose and 30% Avicel PH101 are measured by laser diffraction using a dry powder disperser at a feed rate of 22% and a pressure of 1.2 bar. True densities are obtained from the supplier. Fig. 2-3 illustrates the particle size distribution and Table 2-3 summaries their physical properties. The median diameter of lactose is larger than that of Avicel PH101 while the spans, (D90-D10)/D50=1.923 and 1.860, respectively, are close to each other. Mixing these two materials have little influence on particle size distribution whose

median diameter falls between the raw materials. The median diameter of blends, together with that of granules, can be used to calculate the growth ratio.

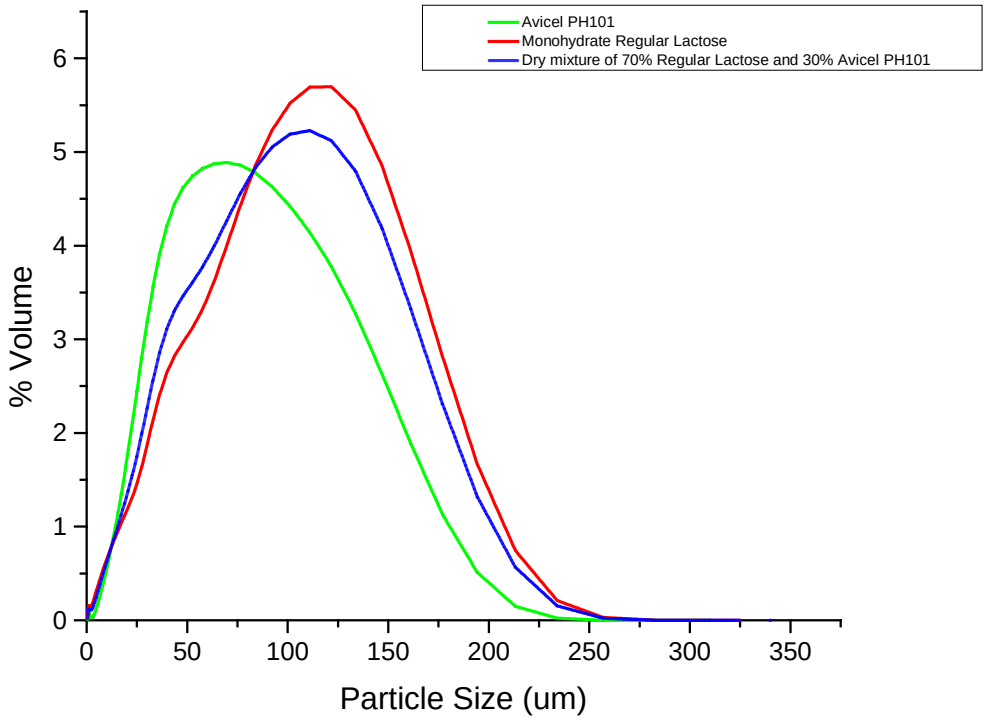

Fig. 2-3 Particle size distribution of raw materials

Table 2-3 Particle size parameters of raw materials

		Avicel PH101	Regular Lactose	Dry Mixture
PSD(um)	D10	19.091	13.738	14.766
	D25	34.173	37.772	34.711
	D50	58.715	78.3543	68.038
	D75	95.176	122.715	110.285
	D90	132.53	159.455	146.229
True Density(g/ml)		1.403	1.543	

2.1.4.2 Penetration Time

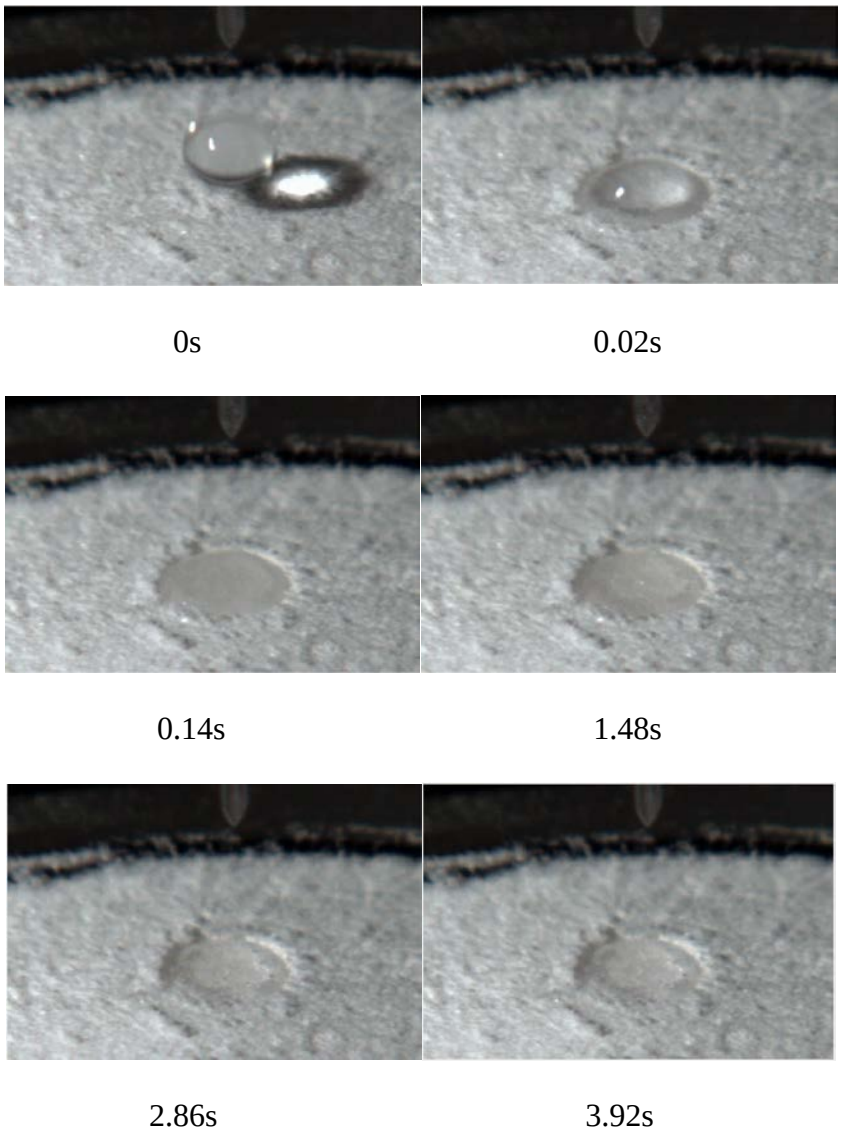

Fig. 2-4 Syringe Penetration Test

For testing penetration time, the powder bed of dry mixture containing 69.3% lactose and 29.7% Avicel PH101 was prepared through Freeman FT4 Powder Rheometer, which generates more reproducible powder bed porosities. A vessel with a diameter of 50 mm was split into an upper 85 mL vessel and a bottom 160 mL vessel. When pouring powder into the split vessel, it was necessary to ensure that powder level was above the split line. Then powders would go through the conditioning step, a rotating blade moving up and down several times through the powder bed, to remove the trapped air or any

preconsolidation history and create a reproducible powder bed. The conditioned powder bed was then slightly compacted and then split to generate an even surface for the single droplet experiments. A high-speed camera was set up and kept recording the penetrating process until there was no significant change in the reflections seen on the powder surface. The penetration time was determined by analyzing the video. A water droplet was released onto the powder bed from a syringe with twenty two gauge needle. The drop size from this syringe can be calculated based on the weight and density of water droplet. With this measurement, penetration time for any other drop size can be determined from the following equation:

$$\frac{t_{p,1}}{t_{p,2}} = \frac{d_{d,1}^2}{d_{d,2}^2} \qquad 2\text{-}1$$

where t_p is the penetration time and d_d is the diameter of a droplet. Finally, drop penetration time was averaged from 10 measurements. [48-49]

As shown in Fig. 2-4, the droplet releasing from syringe took around 3.92 ± 0.76 seconds to completely penetrate into the powder bed. The droplet size of syringe was $5.62 \pm$ 1.81mm while that of nozzle was 11.68 ± 3.38 mm. Therefore, drop penetration time from the nozzle would be 16.94 s. To achieve a good granulation performance, namely granulation in drop controlled region, it is necessary to have a comparable or even larger circulation time to reduce the dimensionless penetration time (see Eq. 1-3). However, measuring the circulation time is difficult because of the determination of flow patterns inside the granulator. The surface velocity of powder is more measurable and circulation time can be estimated through the surface velocity measurements.

For batch processes, the kinetics of drop penetration is mainly controlled by formulation properties while the flux of drops onto the bed surface is largely controlled by process parameters.[18] However, in continuous processes the process parameters can also influence the drop penetration process through the powder residence time. For example, in Table 2-4, the bulk residence time of batch 10 (660RPM and 0.3 L/S ratio) is around 41.4 seconds. According to Eq. 2-1, the droplet size should be around 7.8mm, and any larger droplets cannot completely penetrate into the powder bed when powders approach the granulator outlet. Thus a relatively large mean residence time or small droplet size is desirable, otherwise powders would flow out of the granulator before droplet completely penetrates into the powder bed.

2.1.5 Physical Characterization of Granules

2.1.5.1 Moisture Content

The moisture content was obtained from loss on drying in the fluid bed dryer. Weight of wet granules was recorded once they flowed out of the granulator. The granules were dried for 3 hours under the temperature of 50℃. To ensure the amount of water added into the system is equal to the setting point of L/S ratio, a scale was placed under the water drum to record its weight every 3 minutes for 12 minutes.

2.1.5.2 Particle Size Distribution

Particle size distribution of the dried granules was measured by sieve analysis with an Allen Bradley Sonic Sifter (Allen Bradley, Milwaukee, WI) equipped with a pan and a set of 13 screens-i.e., #US 5 (4000 um), 10 (2000 um), 14(1400 um), 20(850 um), 30(600 um), 40(425 um), 60(250 um), 80(180 um), 100(150 um), 140(106 um), 200(75 um), 270

(53 um) and 400 (38 um). A representative samples of 150g were tested for 30 minutes with a sift setting of 5 and pulse setting of 5.

2.1.5.3 Hold-up Measurement

In continuous processes, the hold-up of granules in the mixer granulator is important as it determines the residence time distribution and thus the total average strain and wet massing time experienced by the granules when they travel through the granulator. Hold-up was measured by simultaneously monitoring the weight of the granules collected at the outlet of the granulator and that of granulating liquid and powder being fed into system. Granules were collected in a collection bucket resting on a scale at the exit of the outlet of the granulator. The amount of the powder being fed was monitored by the in-built scale of loss-in-weight feeders while that of water being fed was monitored according to a scale under the water bucket. The difference between the three weights (weights of water and powder fed into system minus that of granules flowing out) at a given time gives the hold up. In preliminary measurements, hold-up is set as zero at the beginning. It increases gradually with time until it achieves a plateau. The granulator operating under constant hold up was considered to be operating at the steady state. Besides, the hold up measurement can confirm the measurement of mean residence time obtained from the RTD curve. It can be used to calculate bulk residence time (hold-up (kg)/flow rate (kg/h) of the granules in the granulator, thereby reflecting the granules flow behavior inside the granulator.

2.1.5.4 Flow Properties

The FT4 powder rheometer from Freeman Technology (Malvern, Worcestershire, UK) was utilized to test the flow properties of granules. The image and schematic of this shear

cell is shown in Fig. 2-3-1. Basically, there are three operational steps. First, the granules are conditioned by a pass through of a dynamic blade, which can erase powder history and elicit a homogeneous reproducible state. Secondly, the conditioned samples are pre-compacted by applying a normal stress by a vented piston, thereby removing the entrapped air. Finally, the samples are pre-sheared until a steady state flow is reached and then further sheared to acquire a yield point. The responses to characterize granules flow properties are cohesion and Flow Factor (*ff*). Flow Factor is defined as the ratio of consolidation stress in the hopper (major principle stress, σ_1) to the cohesive strength in an arch of exposed surface (unconfined yield strength, σ_c) as presented in Eq. 2-1 When powders start to flow, the stress developed in an arch equals the unconfined yield strength. A larger Flow Factor means a better flow properties because the cohesion between granule particles in the exposed surface of arch is smaller compared with the compacting stress.

$$FF = \frac{\sigma_1}{\sigma_c} \qquad 2\text{-}2$$

Fig. 2-5 The schematic (a) and the image (b) of the shear cell setup supplied with the FT3 Powder Rheometer (Freeman Technology, Inc.)

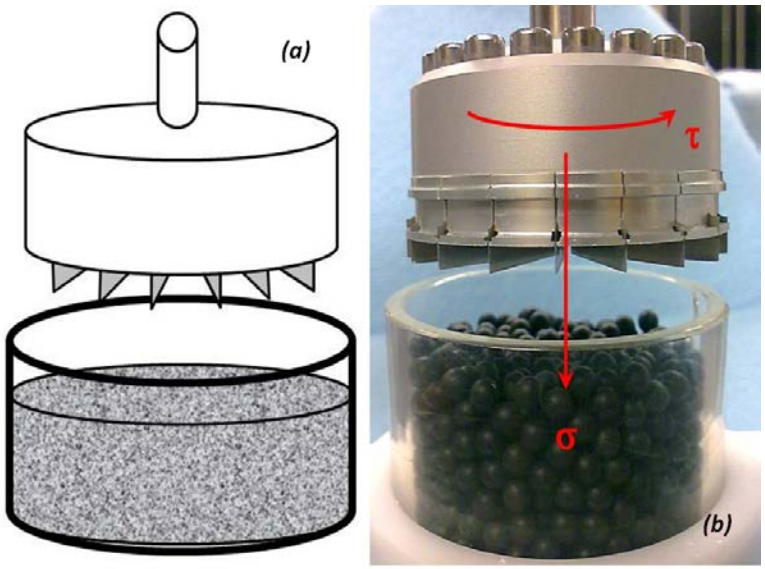

2.1.5.5 Density

Bulk Density is also measured by FT4 powder rheometer. A standardized packing state is achieved by the conditioning process which comprises a traverse of blade downward and then atraverse upward. Therefore, any residual compaction before test can be removed. After spliting the 25mm*10ml vessel, bulk desnity can be calculated based on the recorded weight and volume. Tapped density is measured by an automated tapped density analyzer from Quantachrome Instruments. The volume of standard test cylinder is 250ml. The sample is initially tapped 500, 750 and 1250 times. The volume of tapped sample is checked and another 1250 tap test ensues. This procedure should be repeated if the volume difference between V_{500} and V_{1250} is above 2%. The result is used to calculate tap density according to the sample weight and tapped volume. Then the Hausner Ratio (HR) was calculated from bulk and tapped density with the following equation:

$$HR = \frac{\rho_f}{\rho_i} \qquad 2\text{-}3$$

where ρ_i is the bulk density while ρ_f is the tapped density.

2.1.5.6 Compaction

Tablets were manufactured by the Fette P2100 36 stations. Upper compression force was maintained around 8kN, 10kN, 12kN, 16kN, 20kN and 24kN. The Fette P2100 36 station is a fully instrumented single station tablet press, which can be used to simulate and analyze different phases of tablet press such as pre-compresion, compression and ejection under identical conditions. The punch displacements can be adjusted to realize different dosing amounts. For each tablet, the upper punch compression and pre-compression forces, minimum thickness, ejection force, take-off force and linear speed can also be recorded. A flat-faced round tooling with 10mm diameter was used with direct cam setting. Three 348mg tablets were compressed for each sample. The tablet thickness was measured by Mituyoyo Digimatic thickness gage while the hardness is measured by crushing tablets in Dr. Schleuniger Model 6D tablet tester. Breaking force can be converted into tensile strength by the following equation

$$\sigma_t = \frac{2F}{\pi dh} \qquad 2\text{-}4$$

σ_t is the tablet tensile strength (MPa), F is the tablet break force (N), d and h is the tablet diameter (mm) and thickness (mm), respectively.

2.1.5.7 Particle Shape

The shape of granules were examined by the Eyecon^{TM} 3D high speed imaging camera (Innopharma Labs) at Bench top measurement mode.

2.2 Results and Discussion

Table 2-4 I-optimal design and experimental results

#	Rotation Speed(RPM)	L/S Ratio	Blade Configuration	Nozzle Position	Flow rate(kg/hr)	Moisture Content(%)	PSD						
							D10	D50	D90	Span	%fines(<64um)	Growth Ratio	Hold_Up(g)
1	415	0.2	FB	P1	10	19.26	43.21	93.43	535.63	5.27	0.2211	1.37	51.44
2	415	0.2	FB	P1	10	19.26	42.30	93.04	575.81	5.73	0.2276	1.37	53.84
3	415	0.2	FB	P1	10	19.26	43.78	94.55	558.89	5.45	0.2165	1.39	50.49
4	275	0.3	FB	P2	10	28.97	89.96	198.89	3910.35	19.21	0.0327	2.92	302.31
5	133	0.1	FB	P1	10	9.13	39.08	91.68	204.84	1.81	0.2980	1.35	195.83
6	538	0.3	FB	P1	10	30.02	52.14	136.26	2123.46	15.20	0.1485	2.00	109.46
7	275	0.3	FB	P1	10	30.09	75.69	187.50	3572.12	18.65	0.0626	2.76	273.89
8	133	0.2	FB	P1	10	21.52	58.89	108.04	979.95	8.53	0.1220	1.59	317.41
9	660	0.1	FB	P1	10	9.55	35.37	83.35	213.09	2.13	0.3458	1.23	75.80
10	660	0.3	FB	P1	10	29.27	55.14	141.27	2872.12	19.94	0.1304	2.08	148.83
11	133	0.1	FB	P2	10	11.09	36.17	72.91	140.86	1.44	0.3896	1.07	211.33
12	415	0.1	FB	P2	10	9.27	39.53	81.61	157.85	1.45	0.2769	1.20	49.31
13	415	0.3	FB	P2	10	28.79	47.71	118.02	1946.63	16.09	0.1783	1.73	87.01
14	660	0.3	FB	P2	10	28.28	55.41	141.96	3094.78	21.41	0.1302	2.09	197.83
15	660	0.2	FB	P2	10	18.71	44.78	98.27	815.83	7.85	0.2056	1.44	120.40
16	538	0.2	FB	P2	10	19.83	42.43	96.31	794.73	7.81	0.2224	1.42	93.60
17	275	0.2	FB	P2	10	19.27	41.68	95.52	1010.24	10.14	0.2299	1.40	201.66
18	133	0.2	FS	P2	10	19.27	39.17	89.64	1294.24	14.00	0.2538	1.32	287.35
19	133	0.1	FS	P2	10	13.36	36.42	82.55	289.66	3.07	0.3048	1.21	198.91
20	660	0.1	FS	P2	10	8.36	22.81	81.75	171.49	1.82	0.3545	1.20	77.19
21	660	0.3	FS	P2	10	27.93	45.80	117.52	3397.85	28.52	0.1900	1.73	101.32
22	415	0.3	FS	P2	10	9.39	44.76	117.56	1763.28	14.62	0.1908	1.73	82.40
23	660	0.1	FB	P2	10	19.41	38.88	84.81	162.04	1.45	0.2779	1.25	89.30
24	415	0.2	FB	P2	10	20.64	42.82	89.91	605.07	6.25	0.2333	1.32	68.44
25	415	0.2	FS	P2	10	19.49	47.64	103.31	812.80	7.41	0.1889	1.52	56.37
26	415	0.2	FS	P2	10	19.65	42.48	92.90	944.69	9.71	0.2322	1.37	58.32
27	415	0.2	FS	P2	10	29.34	41.73	90.47	907.00	9.56	0.2423	1.33	58.94
28	275	0.3	FS	P2	10	31.62	49.04	129.31	3063.33	23.31	0.1655	1.90	255.67
29	133	0.3	FS	P1	10	29.63	94.00	201.97	4156.34	20.11	0.0245	2.97	406.75
30	415	0.3	FS	P1	10	29.63	43.01	103.65	2245.47	21.25	0.2142	1.52	70.11
31	660	0.3	FS	P1	10	30.29	47.32	120.09	2979.39	24.42	0.1772	1.77	115.87
32	660	0.1	FS	P1	10	9.67	37.16	81.54	155.70	1.45	0.3077	1.20	64.59
33	275	0.1	FS	P1	10	9.89	37.61	81.12	153.27	1.43	0.3058	1.19	136.81
34	660	0.2	FS	P1	10	19.70	44.06	95.04	832.00	8.29	0.2127	1.40	83.53
35	538	0.2	FS	P1	10	19.71	43.19	97.14	698.06	6.74	0.2164	1.43	77.72
36	415	0.1	FS	P1	10	9.73	38.10	82.15	156.47	1.44	0.2876	1.21	35.22
37	133	0.1	FS	P1	10	9.75	37.95	82.23	159.97	1.48	0.2894	1.21	179.11
38	133	0.2	FS	P1	10	20.86	49.40	97.90	960.25	9.30	0.1780	1.44	255.08

2.2.1 Moisture Content

Moisture content is used to determine if the water distribution during the granulation process is homogeneous. As shown in Table 2-4, the moisture content of all batches are close to their setting points. Therefore, it can be concluded that the distubance from granulation process on water dripping is negligible.

2.2.2 Particle Size Distribution

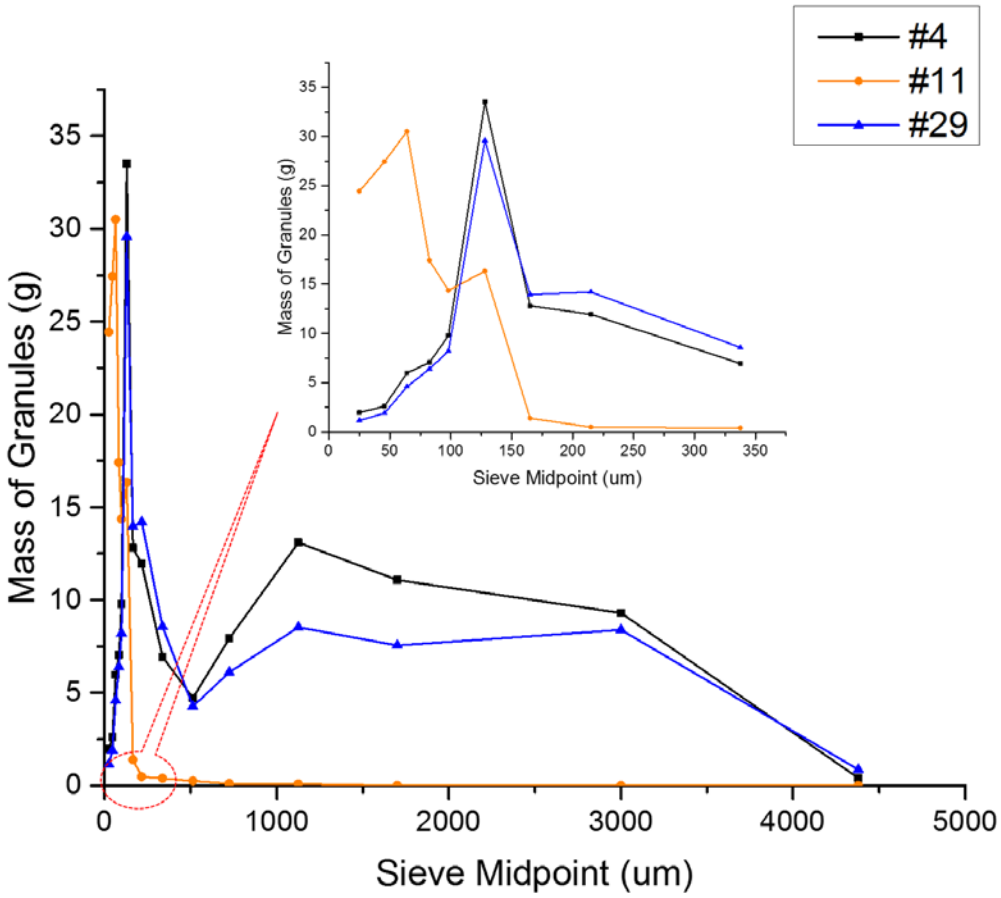

Fig. 2-6 Particle Size Distribution of Granules before Milling

As discribed in section 2.1.5.2, sieve analysis was performed on the unmilled granules after drying. Particle size distribution was calculated based on the weight of the sample on each sieve. The experimental results, together with the DoE, are shown in Table 2-4. Three responses are included in the statistical analysis-i.e., D50, span and percentage of fines. Particle size smaller than 64 microns is defined as fines while that above 1 mm is designated as “lump”. Fig.2-6 shows the particle size distribution of three representative batches. Batch 4 and 29 have the largest D50s (198.89um and 201.97um) while batch 11 has the smallest D50 (72.91um). Before milling, there are substantial amounts of lumps existing in batch 4 and 29, thus widening their particle size distributions. In contrast, batch 11 that consists of more fines has a much narrower distribution.

Table 2-5 shows the ANOVA results for the D50. The statistical significance of each parameter can be determined by either the Pareto chart or the p values. The bar chart shows the t-ratios with blue lines marking a critical value at 0.05 significance. These results depend on the assumption that the Pareto principle applies. That is, most of the variation in any system is generally due to just a few driving factors. Since the first five bars cross the blue line, these factors are statistically significant. Similarly, since the p values of the first five factors are less than 0.05, the same conclusion could be elicited. Specifically, the two process variables and their interaction effects significantly influence the response while the design parameters are not significant. The interaction effect of L/S ratio with blade configuration is also significant. The p value of the quadratic term, L/S Ratio*L/S Ratio, is also less than 0.05, which means that curvature exists in the response surface. From Table 2-4, the majority of D50 values are below 100 microns, indicating that the growth in particle size compared with raw materials is limited. The contour plot, Fig. 2-7, shows that increasing the L/S ratio and simultaneously decreasing the rotation speed can improve the D50 since the residence time of granules are longer at lower rotation speeds. However, powders were inclined to get stuck in the granulator, causing motor overload at the highest L/S ratio and lowest rotation speed because the hold up in the granulator keeps increasing in this case. For instance, at the operation condition of rotation speed 133 RPM and L/S ratio 0.3, the wall of granulator was heating up and finally the shaft was unable to rotate due to the formation of large clumps. When water was used as the granulating fluid, granules would get overwet if the L/S ratio is larger than 30%. The influence of L/S ratio is more significant than rotation speed, which is in

evident in the contour plot. At the highest L/S ratio of 0.3, all batches perform better than other L/S ratios regardless of the rotation speed.

Table 2-5 Analysis of Variance for D50

Term	Estimate	Std Error	t Ratio	Prob>|t|
L/S Ratio(0.1,0.3)	34.642445	3.490502	9.92	<.0001*
Rotation Speed*L/S Ratio	-16.24226	4.444146	-3.65	0.0012*
Rotation Speed(133,660)	-11.78926	3.727268	-3.16	0.0041*
L/S Ratio*L/S Ratio	17.073444	5.441668	3.14	0.0043*
L/S Ratio*Blade Configuration[FS]	-7.486961	3.4031	-2.20	0.0373*
Blade Configuration[FS]	-4.734646	2.614487	-1.81	0.0822
Rotation Speed*Rotation Speed	11.102382	6.252867	1.78	0.0880
Rotation Speed*Nozzle Position[P1]	-3.024796	3.671298	-0.82	0.4178
Nozzle Position[P1]	1.6851909	2.611985	0.65	0.5247
L/S Ratio*Nozzle Position[P1]	2.009352	3.403388	0.59	0.5602
Rotation Speed*Blade Configuration[FS]	1.6961055	3.649314	0.46	0.6461
Blade Configuration[FS]*Nozzle Position[P1]	0.8338561	2.597912	0.32	0.7509

Therefore, it is predictable that conducting the experiments with higher L/S ratio than 0.3 may enhance the granulator performance before granules get overwet or paste is generated.

The growth ratio is defined as the ratio of the final mean diameter of

Fig. 2-7 Contour Plot of D50 versus L/S Ratio and Rotation Speed

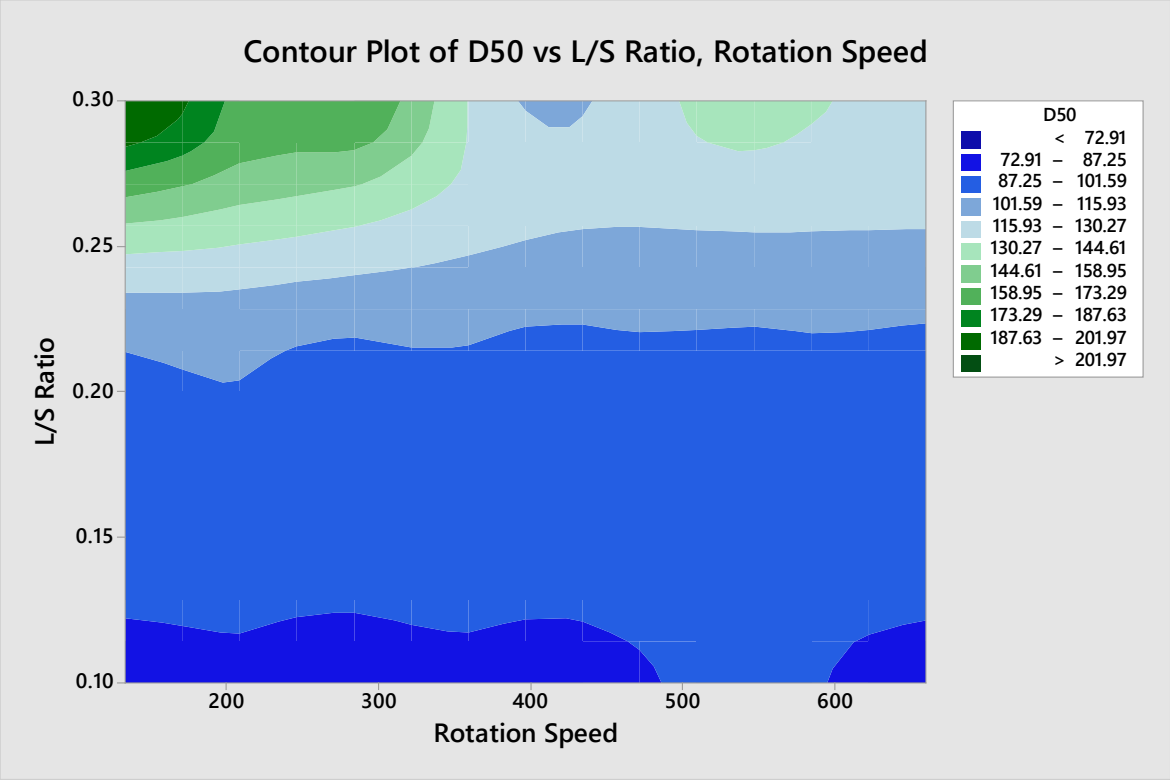

the granules to the initial mean diameter of the dry mixture, thus possessing an identical ANOVA and contour plot with D50. With respect to the percentage of fines, the model includes the same significant terms as the D50 except the quadratic term (see Table 2-6). The percentage of fines is actually proportional to the value of D50-i.e., a higher D50 implies that more powders are granulated during the process. At the operation condition of high rotation speed and low L/S ratio, the percentage of fines is largest (see Fig. 2-8). On one hand, higher rotation speed decreases the residence time of granules. Granules are pushed out of the granulator before they can be sufficiently mixed and granulated. On the other hand, the nozzle used in these experiments is in dripping mode, thus producing droplets with larger size that can take longer to penetrate into the powder bed. Therefore, it is important to strike a balance between the droplet penetration time and granule

residence time. The granulator performance can be improved by using a spray nozzle that generates finer droplet size, which requires less time to penetrate the powder mass.

Table 2-6 Analysis of Variance for % fines

Term	Estimate	Std Error	t Ratio	Prob>|t|
L/S Ratio(0.1,0.3)	-0.097602	0.008007	-12.19	<.0001*
Rotation Speed*L/S Ratio	0.0280438	0.010194	2.75	0.0109*
Rotation Speed(133,660)	0.0233107	0.00855	2.73	0.0115*
L/S Ratio*Blade Configuration[FS]	0.0172846	0.007806	2.21	0.0362*
Rotation Speed*Nozzle Position[P1]	0.0165809	0.008421	1.97	0.0601
Nozzle Position[P1]	-0.009971	0.005991	-1.66	0.1086
Rotation Speed*Rotation Speed	-0.020248	0.014343	-1.41	0.1704
Blade Configuration[FS]	0.0084	0.005997	1.40	0.1736
L/S Ratio*L/S Ratio	0.0132589	0.012482	1.06	0.2983
Blade Configuration[FS]*Nozzle Position[P1]	-0.005085	0.005959	-0.85	0.4016
L/S Ratio*Nozzle Position[P1]	-0.002529	0.007807	-0.32	0.7486
Rotation Speed*Blade Configuration[FS]	0.0003697	0.008371	0.04	0.9651

Fig. 2-8 Contour Plot of % fines versus L/S Ratio and Rotation Speed

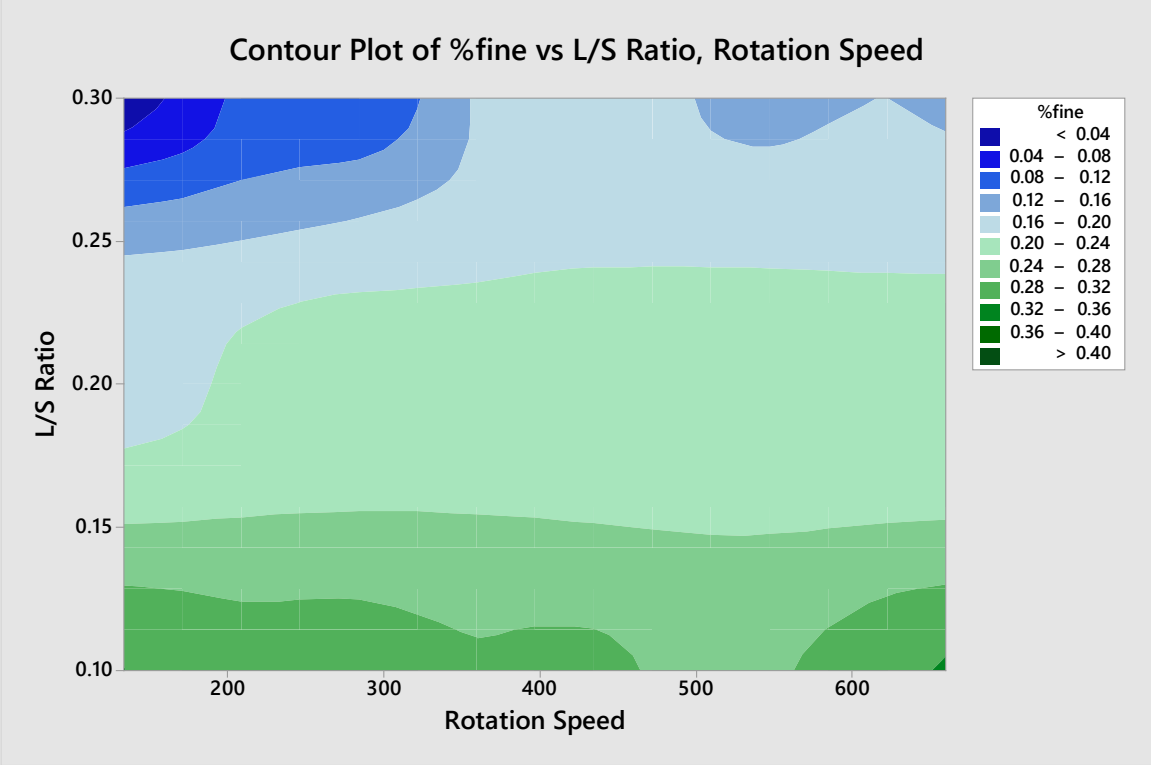

Finally, as shown in Table 2-7, L/S ratio is the only significant parameter that spans the width of particle size distribution. Typically, a span value less than 1 is desirable and represents a relatively narrow distribution. In Fig. 2-9, the particle size distribution becomes wider with increasing L/S ratio. Some spans are larger than 5, indicating that these granulation processes are in the mechanical dispersion regime instead of the drop controlled regime.

Table 2-7 Analysis of variance for Span

Term	Estimate	Std Error	t Ratio	Prob>|t|
L/S Ratio(0.1,0.3)	10.248122	1.731553	5.92	<.0001*
Rotation Speed*Nozzle Position[P1]	2.6981875	1.821241	1.48	0.1510
L/S Ratio*Blade Configuration[FS]	2.4756692	1.688195	1.47	0.1550
Blade Configuration[FS]	1.7716583	1.296983	1.37	0.1841
Nozzle Position[P1]	-1.541349	1.295742	-1.19	0.2454
L/S Ratio*L/S Ratio	2.8530376	2.699479	1.06	0.3007
Rotation Speed*L/S Ratio	1.8366286	2.204632	0.83	0.4127
L/S Ratio*Nozzle Position[P1]	-0.97326	1.688338	-0.58	0.5695
Blade Configuration[FS]*Nozzle Position[P1]	0.5571561	1.288761	0.43	0.6692
Rotation Speed*Blade Configuration[FS]	-0.427724	1.810335	-0.24	0.8151
Rotation Speed(133,660)	0.1387281	1.849007	0.08	0.9408
Rotation Speed*Rotation Speed	0.0686482	3.101894	0.02	0.9825

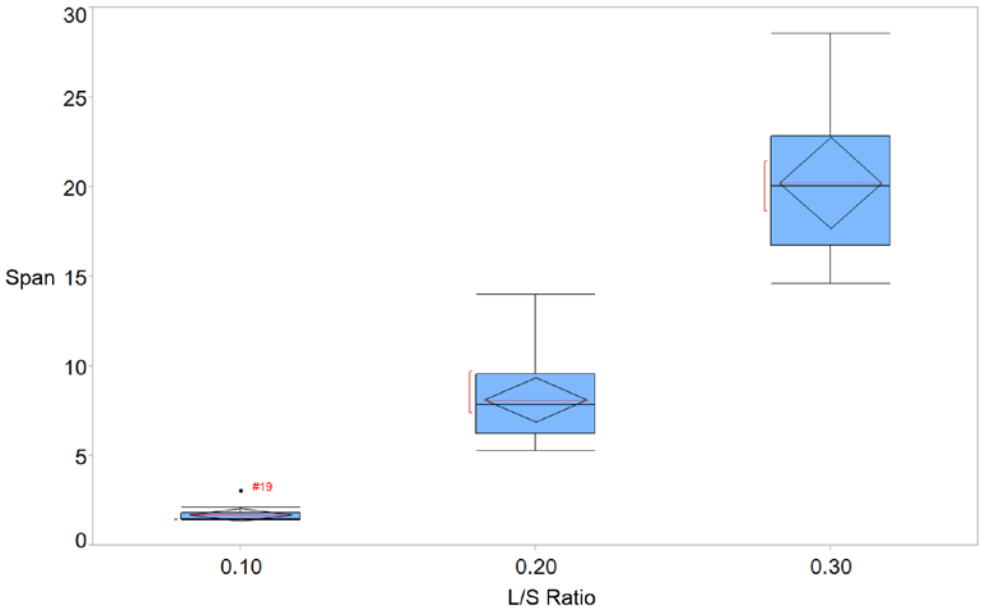

Fig. 2-9 Relationship between Span and L/S Ratio

2.2.3 Hold-up and Shear

Table 2-8 indicates that the main effects of rotation speed, L/S ratio and blade configuration are statistically significant in affecting the hold up. Also, the interaction effect between rotation speed and L/S ratio as well as the curvature effect of rotation speed*rotation speed will make a difference in hold up measurement. As shown in Fig. 2-10, and Fig. 2-11, for all L/S ratios and blade configurations, the hold up first decreases, reaches a minimum value and then increases with the increase of rotation speed. Also, this effect becomes more apparent as the L/S ratio changes from 0.1 to 0.3. Since the flow rate is constant (10 kg/hr), the mean residence time is proportional to the holdup. At low rotation speed (<400rpm), granules are pushed out of the mixer faster with increase in the RPM, leading to a lower holdup and less amount of mechanical work (total strain). Adding more granulating liquid, namely increasing L/S ratio, can compensate for the decrease of hold up. At high rotation speeds (>400RPM), the powder bed is operated at a nearly fluidized state, and wet granules can be further densified by increasing the RPM, leading to higher hold up. In this continuous system, mixing tools (blades and shaft) generate a mechanical fluid bed when the rotation speed is high. When granulating liquid was added to the primary particles in the fluid bed, they were broken up and homogeneously distributed in the material due to the mixing mechanism. Subsequently the intense mixing process induced multitudinous contacts among particles and droplets. The adhesive force thus came into effect and binded together primary particles to form agglomerates, which were further densified and indurated due to the significant collision between particles, mixing tools and granulator wall.

If the rotation speed is high, the FB blade configuration can have more hold up because it creates backward mixing and recirculating zones in the granulator, which increases the bulk residence time and the influence of blade configuration diminishes with a decrease in rotation speed, indicating that the granulator capacity becomes the limiting parameter. [50] When hold up is fairly close to the granulator capacity, flow problems will occur and powders cannot be thoroughly exposed to liquid, thereby impacting adversely on the granulation process or even lead to motor overload.

Moreover, the shear intensity (strain) applied on the granules can be evaluated by the number of blades passes, i.e., the total number of revolutions that granules encounter in the granulation systems. It is important to estimate the total strain that particles undergo during the granulation process because it can affect granule flow behavior, porosity, bulk density and content uniformity. All of these are essential attributes of granules. The total strain is calculated as the product of bulk residence time (hold up divided by water and dry powder flow rates) and rotation speed. In general, larger blade passes indicate better granulation and mixing performance at a constant hold up. In table 2-9, the main effects of rotation speed, L/S ratio and blade configuration are statistically significant in affecting the energy input. Besides, the curvature effect of rotation speed* rotation speed also makes a difference in hold up measurement, thereby necessitating a second order model to predict the energy input. In Fig. 2-12 and Fig. 2-13, two maximum peaks can be found at 275RPM and 660 RPM. This is in accordance with the outcome of particle size distribution-i.e., D50s under these rotation speeds are larger than any other operation conditions. Therefore, in terms of this Glatt continuous high shear granulator, the optimum operation condition is 0.3 L/S ratio with a rotation speed of 275RPM or

660RPM. Rotation speed above 660 RPM is beyond the capability of this granulator, hence 275 RPM was deemed the optimal value.

Table 2-8 Analysis of Variance for Hold-up

Term	Estimate	Std Error	t Ratio	Prob>|t|
Rotation Speed(133,660)	-0.104233	0.007809	-13.35	<.0001*
Rotation Speed*Rotation Speed	0.1294937	0.013101	9.88	<.0001*
L/S Ratio(0.1,0.3)	0.0609413	0.007313	8.33	<.0001*
Rotation Speed*L/S Ratio	-0.043405	0.009311	-4.66	<.0001*
Blade Configuration[FS]	-0.01142	0.005478	-2.08	0.0475*
L/S Ratio*Blade Configuration[FS]	-0.011072	0.00713	-1.55	0.1330
Blade Configuration[FS]*Nozzle Position[P1]	0.0077497	0.005443	1.42	0.1669
Nozzle Position[P1]	-0.006843	0.005472	-1.25	0.2227
L/S Ratio*L/S Ratio	0.0086071	0.011401	0.75	0.4573
L/S Ratio*Nozzle Position[P1]	-0.002781	0.007131	-0.39	0.6998
Rotation Speed*Blade Configuration[FS]	0.0020953	0.007646	0.27	0.7863
Rotation Speed*Nozzle Position[P1]	0.0005585	0.007692	0.07	0.9427

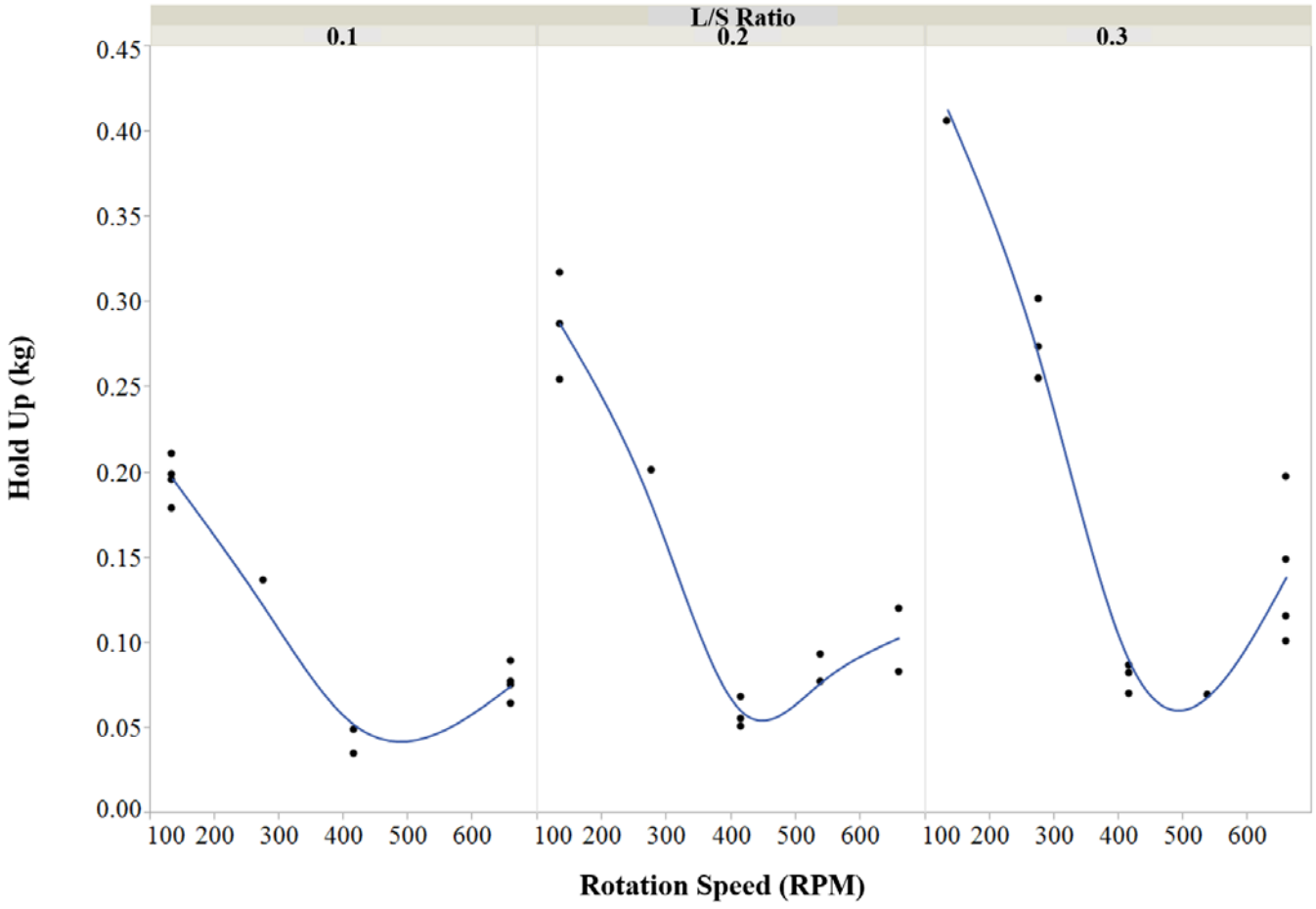

Fig. 2-10 Effects of L/S Ratio and Rotation Speed on Hold-up

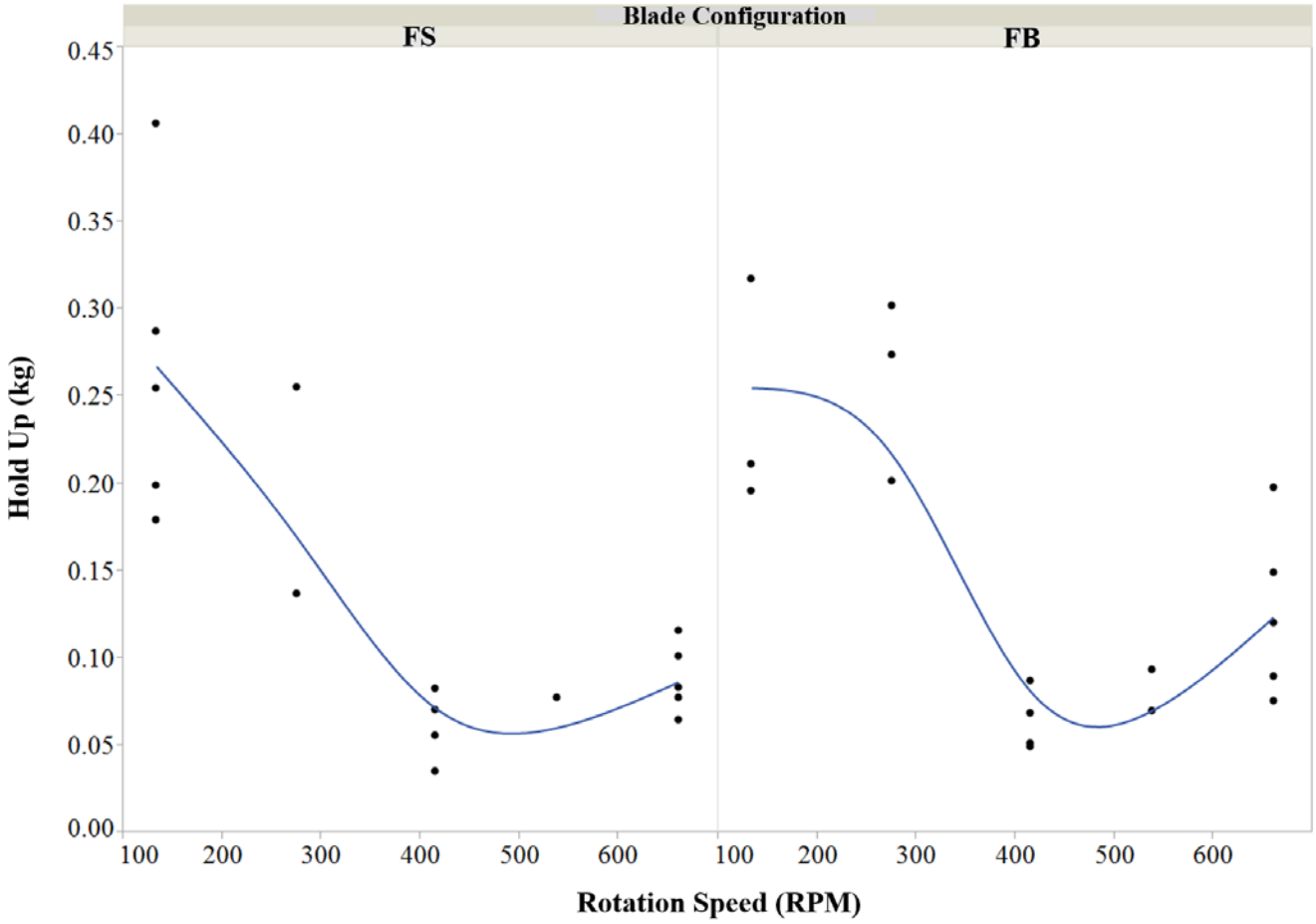

Fig. 2-11 Effects of Blade Configuration and Rotation Speed on Hold Up

Table 2-9 Analysis of Variance for Shear

Term	Estimate	Std Error	t Ratio	Prob>|t|
Rotation Speed*Rotation Speed	147.28365	27.11979	5.43	<.0001*
L/S Ratio(0.1,0.3)	75.089648	15.13892	4.96	<.0001*
Rotation Speed(133,660)	43.584574	16.16582	2.70	0.0124*
Blade Configuration[FS]	-26.11208	11.33949	-2.30	0.0299*
Nozzle Position[P1]	-20.89975	11.32864	-1.84	0.0769
L/S Ratio*Blade Configuration[FS]	-26.21356	14.75985	-1.78	0.0879
Blade Configuration[FS]*Nozzle Position[P1]	14.761071	11.2676	1.31	0.2021
L/S Ratio*L/S Ratio	25.319246	23.60148	1.07	0.2936
Rotation Speed*L/S Ratio	-20.05415	19.27505	-1.04	0.3081
L/S Ratio*Nozzle Position[P1]	-14.37175	14.7611	-0.97	0.3396
Rotation Speed*Blade Configuration[FS]	-5.761479	15.82772	-0.36	0.7189
Rotation Speed*Nozzle Position[P1]	-0.920536	15.92307	-0.06	0.9544

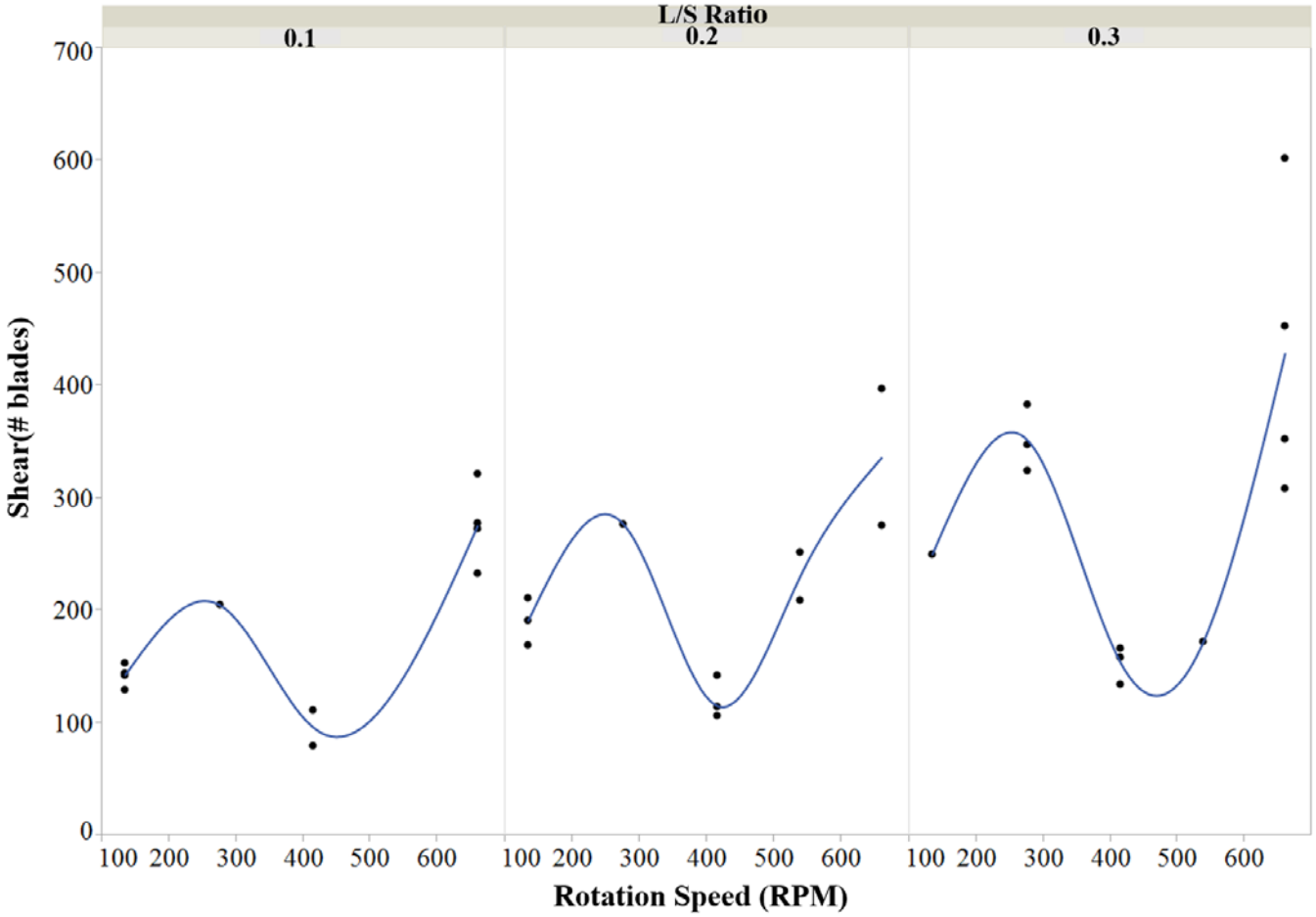

Fig. 2-12 Effects of L/S Ratio and Rotation Speed on Shear

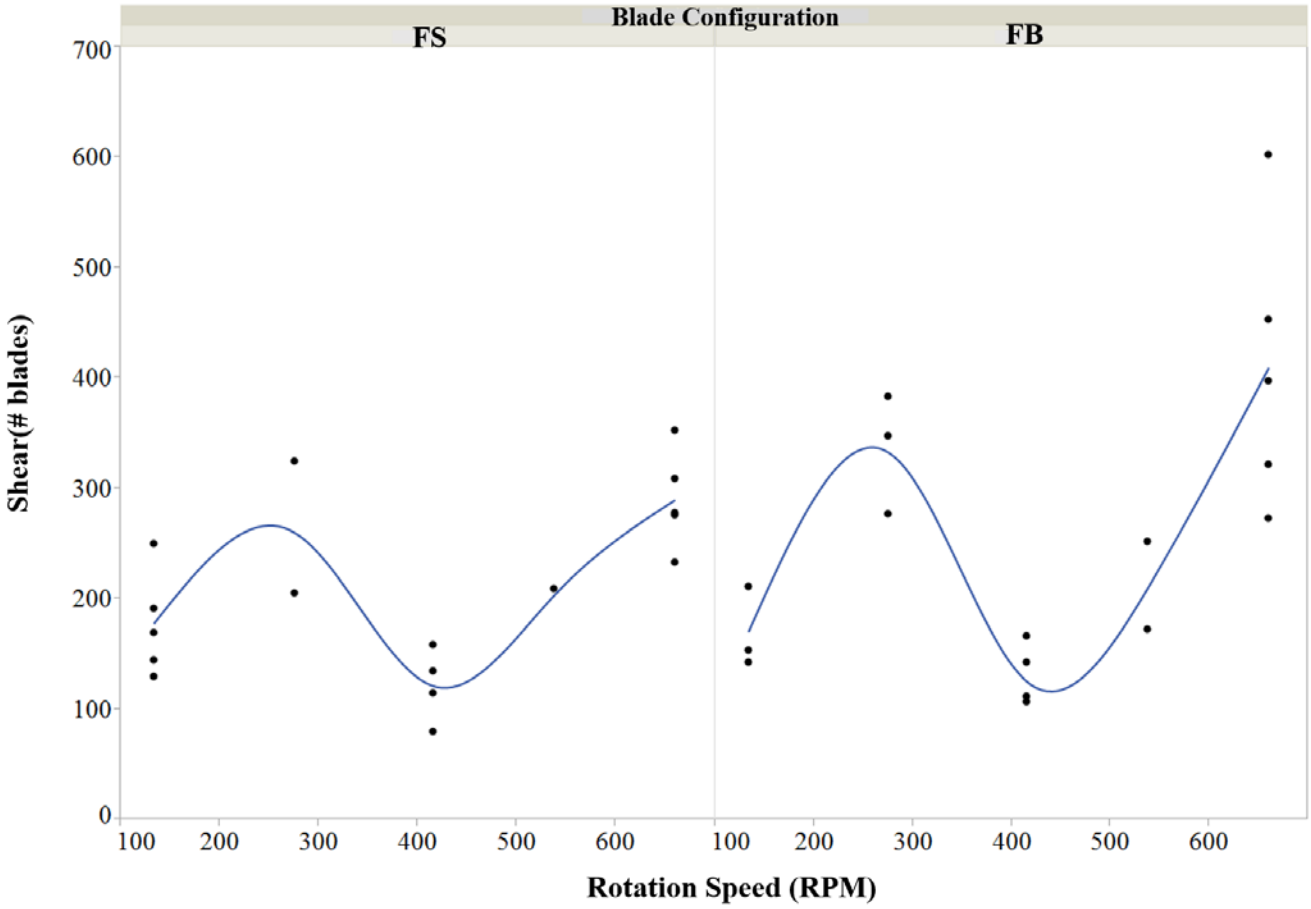

Fig. 2-13 Effects of Blade Configuration and Rotation Speed on Shear

2.2.4 Flow Properties

Based on the measurement results of particle size distribution, 8 batches with relatively large D50 were selected for further characterization, since typically the most important property attribute of granules is its particle size distribution. As mentioned before, the selected granules were milled and then mixed with 1% Magnesium stearate in a LabRAM mixer from Resodyn Acoustic Mixers. The characterization results of the flowability of the final blends are shown in Table 2-11. The points generated at different normal stress, σ_{Ni} ,and shear stress, τ_{Ni} , were plotted in $\sigma - \tau$ space to depict the failure yield locus by FT4 powder rheometer, which represents the moment when powder flow is initiated. All

samples were subject to a pre-consolidation stress of 3kPa (σ_N). The Mohr stress circle analysis was utilized to calculate the values of major principles stress, σ_1, and unconfined yield strength, σ_c, as shown in Fig. 2-13 that takes #14 as an example. The values of cohesion were obtained from the intercept of the linearized yield locus to the shear stress axis. The pair of $\sigma_1 - \sigma_c$ values was then plotted as a point to represent granules flow function, namely the relationship of $\sigma_c = f(\sigma_1)$. According to the Jenike classification of Bulk Flow Behaviour, flowability can be divided into five different regions in terms of flow factor values, namely not flowing, very cohesive, cohesive, easy-flowing and free-flowing (see Fig. 2-14). In this study, the highest flow factor is 14.639 while the smallest flow factor is 7.842. Therefore, all granule batches are at least easy or free flowing characteristic. Significant flowability differences cannot be detected especially for those values around or even above 10. A better granulation performance with a high D50 and low percentage of fines is conducive to decreasing the unconfied yield strength-i.e., the powders are likely to flow more easily. Since all selected samples were collected under the L/S ratio of 0.3, this observation means that it is necessary to maintain a high level of water amount for the purpose of improving powder flowability. Also, in the continuous granulator, the energy input was provided by rotating the impeller. Typically, high shear granulation can enhance the mixing performance as well as the granule flowability. Since the strain that granules experience in the granulator is proportional to the product of rotation rate and residence time, it is important to strike a balance between these two terms to maximize the number of blade passes.

Table 2-10 Flow Properties of Selected Batches

Batch #	Cohesion, kPa	UYS, kPa	MPS, kPa	FF

4	0.162	0.582	5.633	9.674
6	0.137	0.510	5.303	10.393
7	0.119	0.435	5.033	11.602
10	0.104	0.380	5.187	13.660
14	0.196	0.682	5.393	7.903
28	0.186	0.665	5.214	7.842
29	0.093	0.349	5.112	14.639
31	0.125	0.477	5.331	11.225

Fig. 2-14 Flow Function and Yield Locus for the Selected Samples

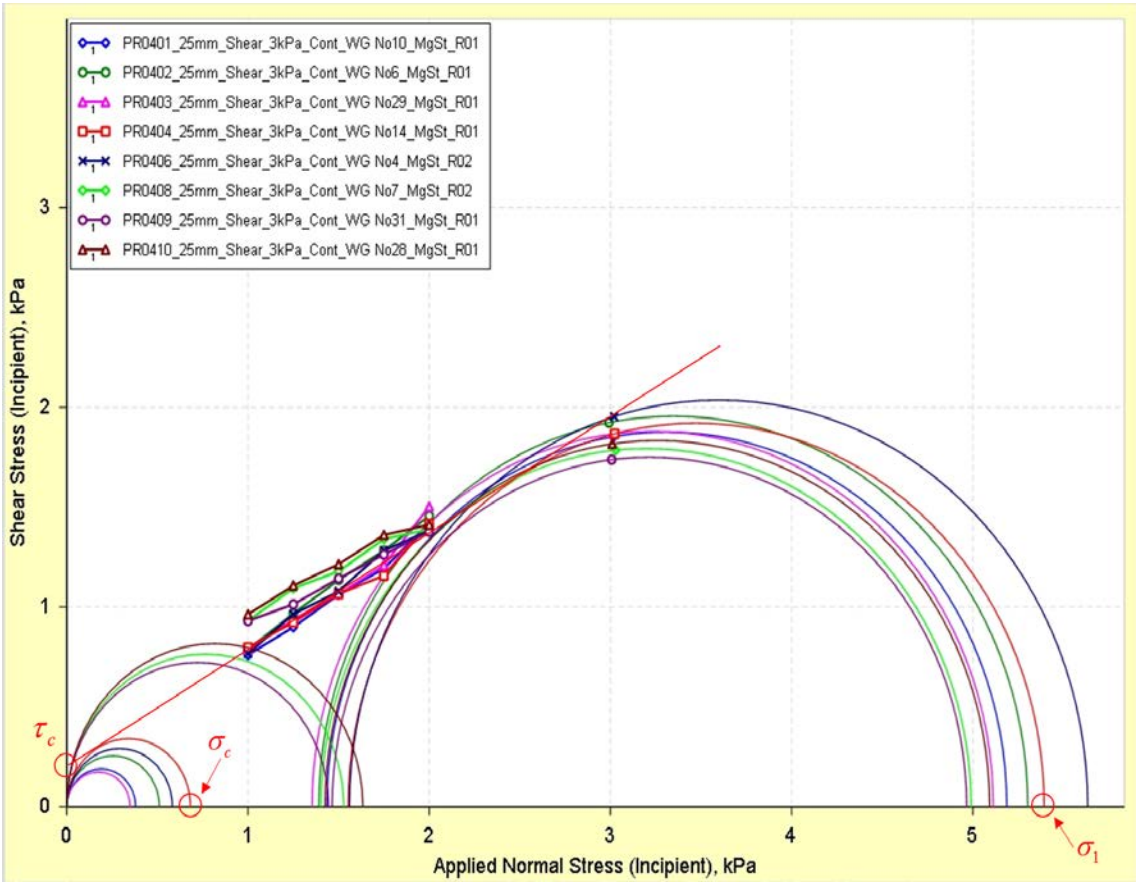

Fig. 2-15 Flowability of Different Samples according to Jenike Classification of Bulk Flow Behaviour

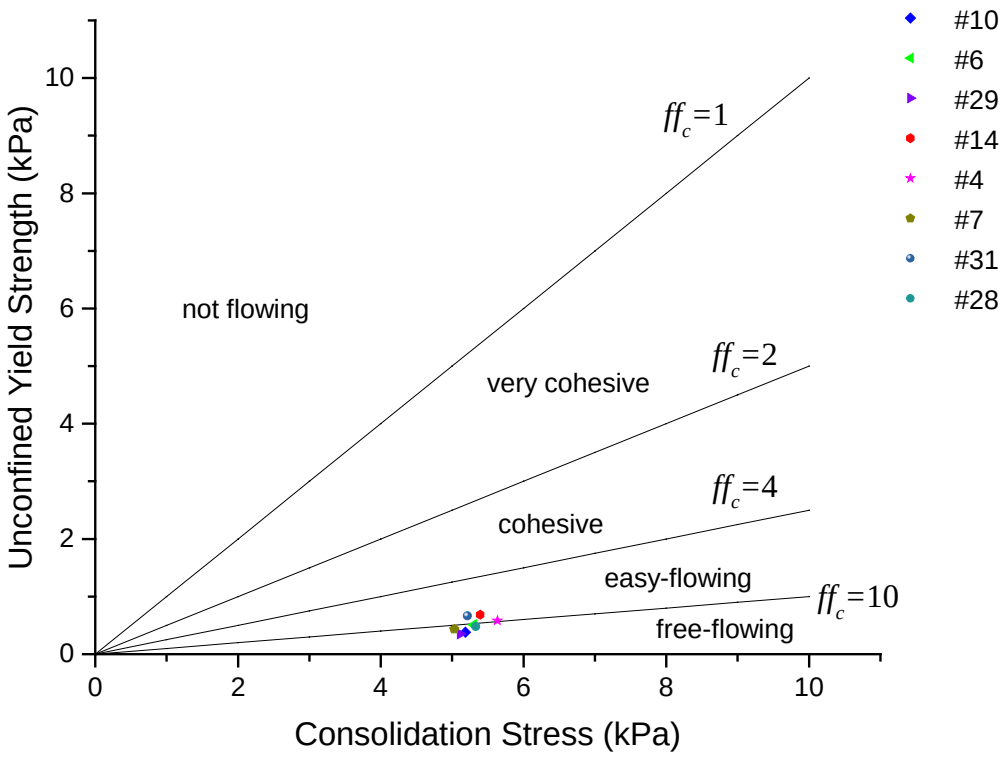

2.2.5 Density

Fig. 2-16 Density of selected batches

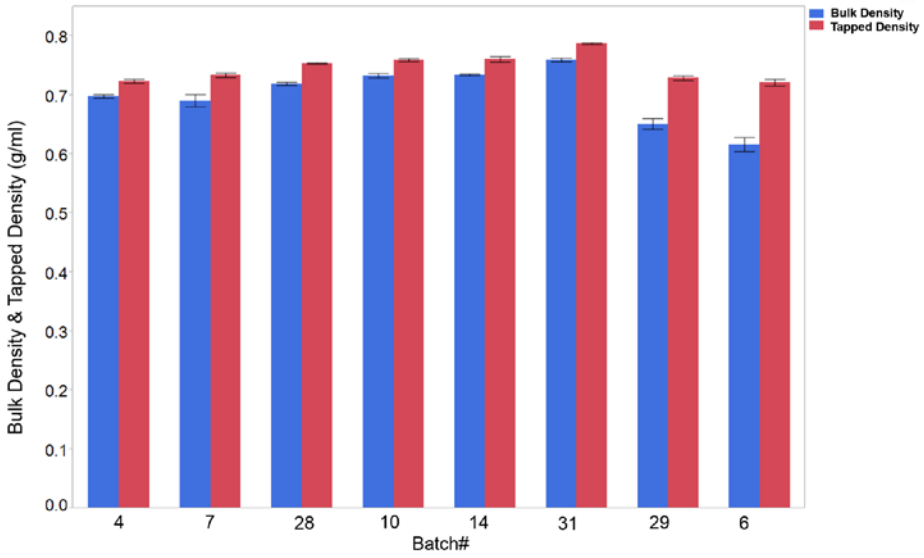

The results for bulk densities of granules ranged from 0.608 to 0.759 g/ml while the tapped densities varied from 0.716 to 0.789 g/ml (see Fig. 2-16). Hausner ratio values were calculated from the bulk and tapped densities to describe the flowability of the granules. Hausner ratio can be interpreted according to the range described in USP Powder flow <1174>. When Hausner ratio falls into the range of 1.00-1.11, it indicates that flowability of powder is excellent. When the Hausner ratio falls into the range of 1.12-1.18, it indicates that the flowability of powder is good. As a result, flowability of all batches are either excellent or good, which is in accordance with the flow factor test results by FT4 powder rheometer.

2.2.6 Compaction

Table 2-11 Operation Conditions of Selected Batches

#	Rotation Speed(RPM)	L/S Ratio	Blade Configuration	Nozzle Position	Flow rate(kg/hr)
4	275	0.3	FB	P2	10
7	275	0.3	FB	P1	10
10	660	0.3	FB	P1	10
14	660	0.3	FB	P2	10
28	275	0.3	FS	P2	10
31	660	0.3	FS	P1	10

All the selected 6 batches were firstly used to manufacture tablets under the compression force of 10KN. For convenience, the operation conditions are again shown in Table 2-11. The tablets data including thickness, weight and hardness are shown in Table 2-12. Compression force and powder amount are two crucial parameters that can influence the tablets mechanical properties. To make the hardness data from different batches more comparable, the powder weight was controlled around 0.35g.

Table 2-13 shows the particle size distribution of granules after milling. To illuminate the difference of hardness in these batches, Fig. 2-16 presents the relationship between tablets hardness and D50. Overall, with the increase of D50, hardness will decrease. The granules with larger D50 usually produce tablets with larger porosity that are easier to break during the hardness test. Granules with smaller D50 contains more irregular particles, which tend to hook to each other leading to stronger inter-particle bonds during the tablet compaction. Moreover, a process called over-granulation will be induced when granules substantially lose the capabilities of being compressed into tablets with sufficient strength.[47] Typically, these cases occurr if the granulating liquid is excesive thus giving rise to uncontrolled growth to form large granules or if hard and densified pellets are formed on account of the severe collision between granules and blades or granulator wall under high rotation speed. Therefore, it is reasonable to infer that over-granulation occurred in the batches with large D50. Although batch 10 and 14 have similar particle size distribution, remarkable difference exist in their tablets hardness because the high rotation speed 660RPM of batch 10 and 14 tends to bring about over-granulation. Batch 31 has a large tablet hardness, which can be ascribed to the small D50 that counteract the influence of high rotation speed to some extent. Another instance lies in batch 31 and 28, which have almost the same D50 but different tablet hardness. The high rotation speed 660 RPM with batch 31 has intenser densification or consolidation process, thereby leading to a smaller tablet hardness.

Table 2-12 Tablets Data with the upper compression force of 10KN

Batch #	Actual Compression Force (KN)	Thickness(mm)	Weight(g)	Hardness(KPa)
4	10.1	3.35	0.3488	4.3

	10.4	3.38	0.3501	4.4
	10.2	3.32	0.3497	4.6
7	10.2	3.34	0.3491	4.8
	10.2	3.33	0.349	4.7
	10.1	3.31	0.346	4.8
10	9.8	3.25	0.3495	4.8
	9.9	3.26	0.3487	4.5
	10.1	3.28	0.3502	4.8
14	10.3	3.33	0.3521	4.9
	10	3.32	0.3492	4.7
	9.9	3.34	0.3483	4.7
28	9.6	3.32	0.3451	6.1
	9.7	3.29	0.343	6.3
	9.9	3.31	0.3443	6.6
31	10.2	3.31	0.3459	6
	10	3.32	0.3454	5.5
	9.9	3.33	0.3477	5.6

Table 2-13 Particle Size Distribution of Granules after Milling

Batch #	D10	D25	D50	D75	D90
4	47.85	84.26	127.19	194.08	489.87
7	34.83	70.36	111.31	160.78	290.20
10	28.54	57.76	98.07	147.01	231.73
14	32.12	61.88	103.73	163.19	443.30
28	20.54	46.61	86.24	135.48	194.77
31	22.06	48.53	86.38	130.36	176.14

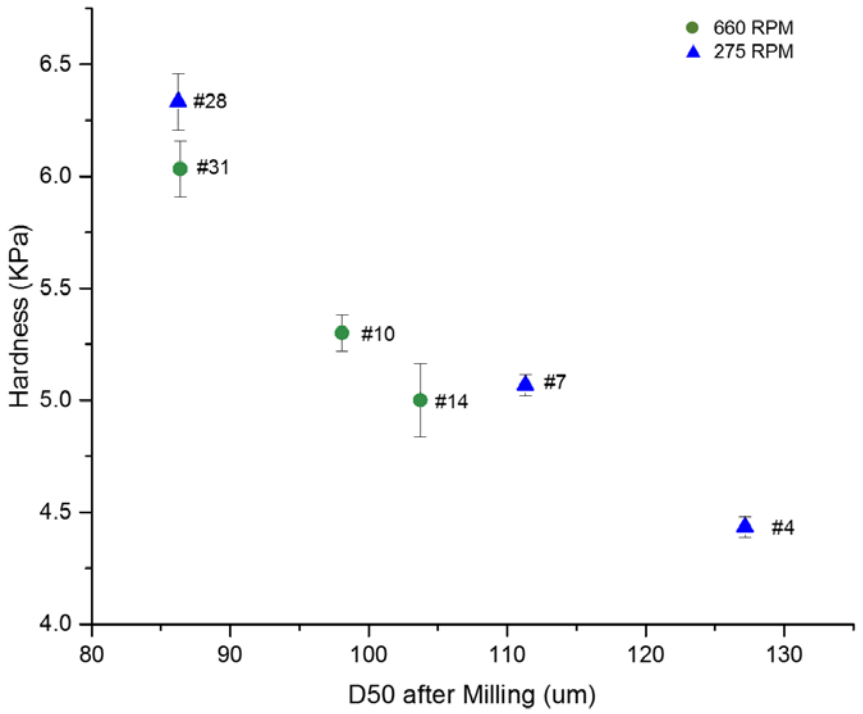

Fig. 2-16 Relationship between Hardness and D50

Table 2-14 Tablets Data for batch #4

Setting Compression Force (KN)	Actual Compression force (KN)	Thickness(mm)	Weight (g)	Hardness(KPa)
8	7.9	3.47	351.8	2.9
	7.9	3.47	352.3	2.8
	7.9	3.47	351.4	2.8
12	12.2	3.32	354	5.1
	12	3.27	349.6	5.1
	12.3	3.28	353.2	5
16	16	3.27	353.6	6.6
	16.3	3.24	356.4	6.9
	16	3.23	355.7	6.8
20	20	3.16	353.3	8.4
	20.1	3.12	351.5	8.1
	20.1	3.14	354.5	8.4
24	23.9	3.09	350.4	8.9
	24.1	3.15	355.6	8.7
	23.7	3.11	352.1	9

Table 2-15 Tablets Data for batch #14

Setting Compression Force (KN)	Actual Compression Force (KN)	Thickness(mm)	Weight (g)	Hardness(KPa)
8	8.1	3.39	347.7	3.1
	7.9	3.41	348	3.1
	8.1	3.43	351.4	3.2
12	11.8	3.24	347.1	5
	12.3	3.21	348.9	5.1
	11.7	3.21	345.2	5.1
16	16.1	3.2	353.7	6.8
	16.1	3.22	356	6.9
	15.7	3.2	352	6.7
20	20	3.12	352.2	7.9
	19.7	3.12	350.9	8.1
	19.7	3.11	350.1	8
24	24.3	3.14	352.5	8.8
	24.2	3.16	354.1	9.3
	24.1	3.13	354.9	8.4

Since the rotation speeds of 275 RPM and 660 RPM produce a more desirable PSD, hold up and shear, granules from batch 4 and 14 were further selected to test their compactability, which is defined as the initial slope of tensile strength versus compression force curve. The tablet property information of batch 4 and 14 is shown in Table 2-14 and Table 2-15. Besides compression force of 10KN, tablets were manufactured under the compression forces of 8KN, 12KN, 16KN, 20KN and 24KN and then went through hardness test. As shown in Fig. 2-17 and Fig. 2-18, granules of batch 4 is slightly more compressible than that of batch 14, which was evident from its larger slope. According to the regime map proposed by Iveson et al. (1998) [19], Stokes' deformation number and maximum pore satuation number determine the category of granulation. Pandey et al. (2013) [51] indicated that there was a strong correlation between granule porosity and compactability and that water amount was the most influential factor with respect to compaction characteristics. Granules are more compressible with the

increase of porosity, which is adversely proportional to granulating liquid amount and pore saturation. Batch 4 and 14 have the same L/S ratio, thereby very close compactability. However, the rotation speed of batch 14 660RPM will produce granules with smaller porosity because of the consolidation or densification during granulation process, i.e., a relatively small slope compared with Batch 4.

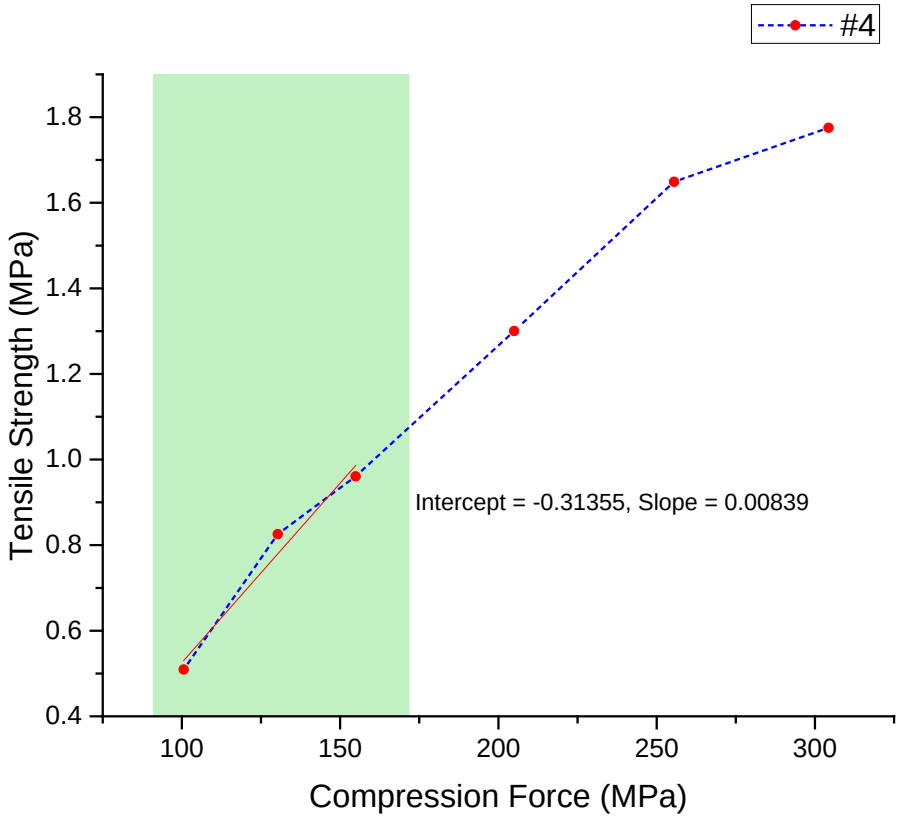

Fig. 2-17 An illustration of compactability for #4

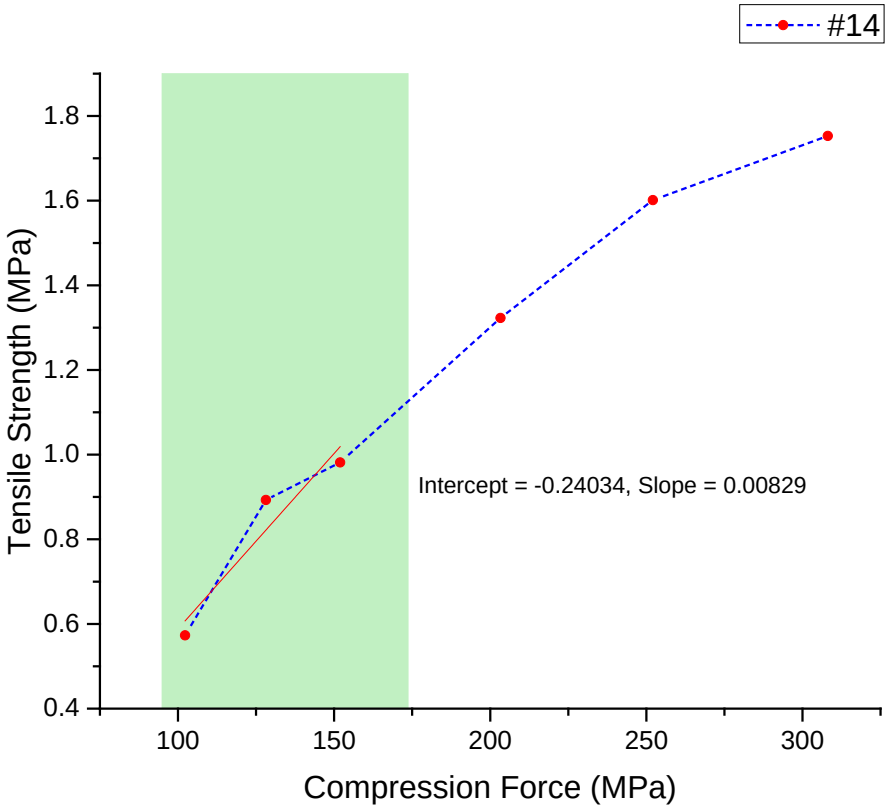

Fig. 2-18 An illustration of compactability for #14

2.2.7 Particle Shape

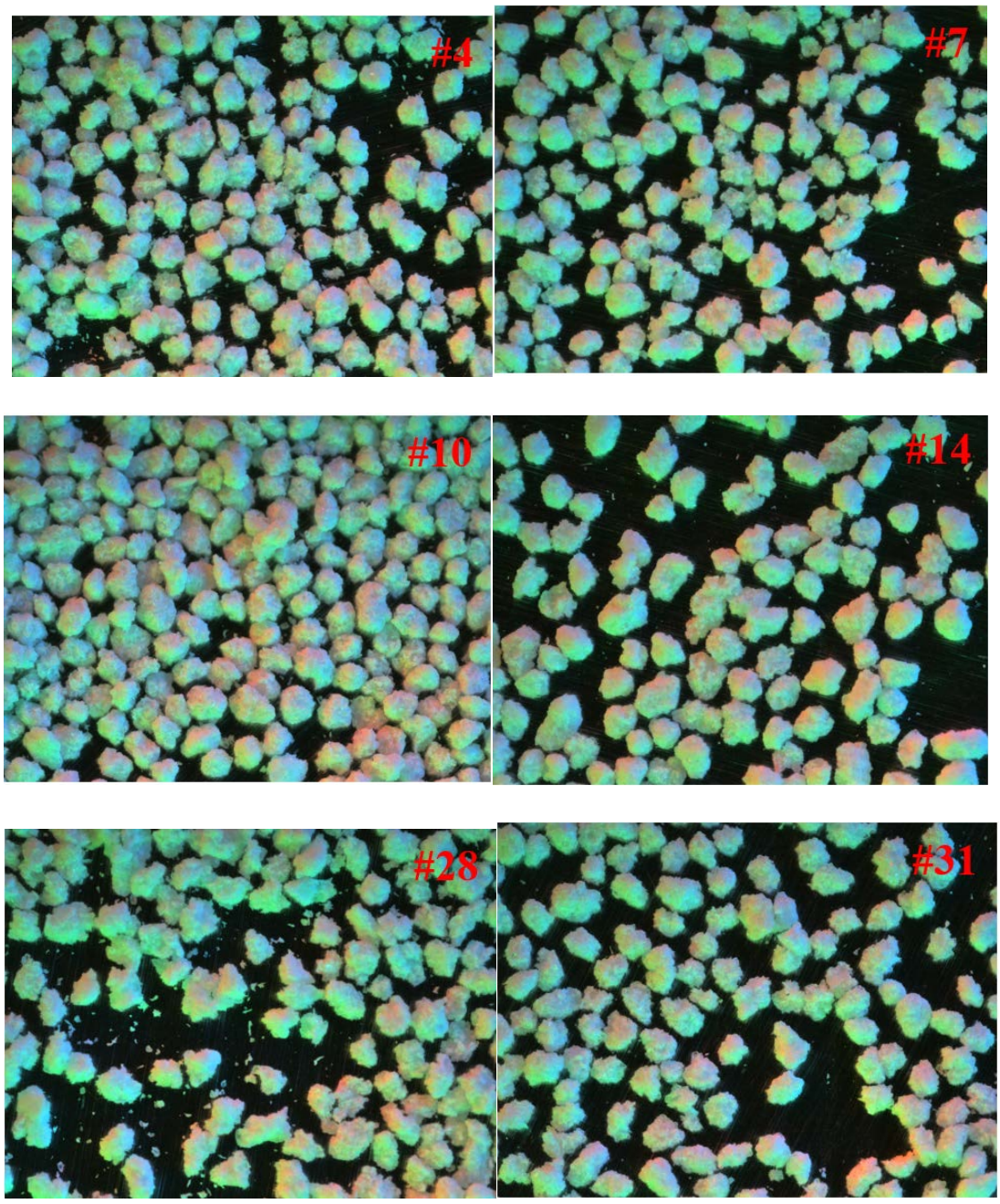

Fig. 2-19 Granules within the size range of 420-595 microns for selected batches

The range of granule size selected for shape characterization is from 420 to 595 microns, which is the most desirable size range after granulation process.[52] As shown in Fig. 2-19, the sphericity of granules from all batches are quite similar to each other. This may be due to the shear forces applied on granules during sieving process, making all granules

more spherical. However, based on Fig. 2-19, some batches such as 4 and 28 contain more small granules while others contain less. These can be attributed to consolidation or densification of batch 10, 14 and 31 with high rotation speed 660RPM, thus making these granules stronger, smoother and more sustainable to extra forces.

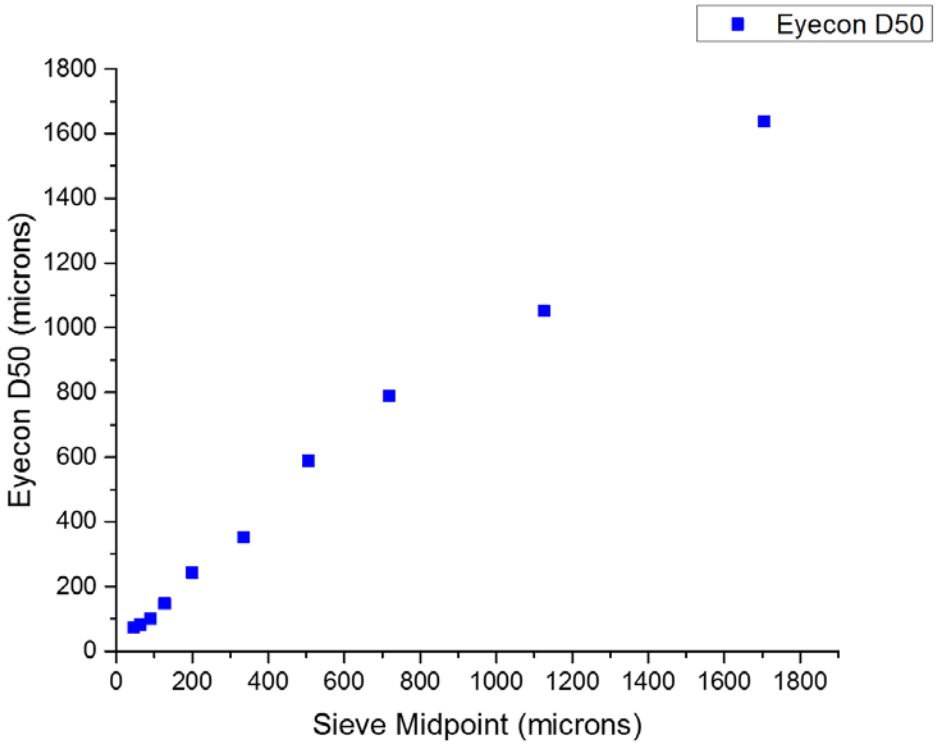

Fig. 2-20 Correlation between eyecon camera and sieve analysis

Since the Eyecon camera is quite suitable for in line monitoring of particle size distribution during the granulation process, its performance was calibrated by sieve analysis. As shown in Fig. 2-20, the particle size distribution of batch 28 was measured by both the Eyecon camera and sieve analysis. It was shown that the Eyecon camera showed good correlation ($R^2 = 0.98$) with sieve measurement for in-line settings, thus demonstrating its sensitivity to process perturbations and potential capabilities for use in process control. Fig. 2-21 shows its size measurement threshold, which is able to accurately capture the particle size ranging from around 50 to 3000 microns.

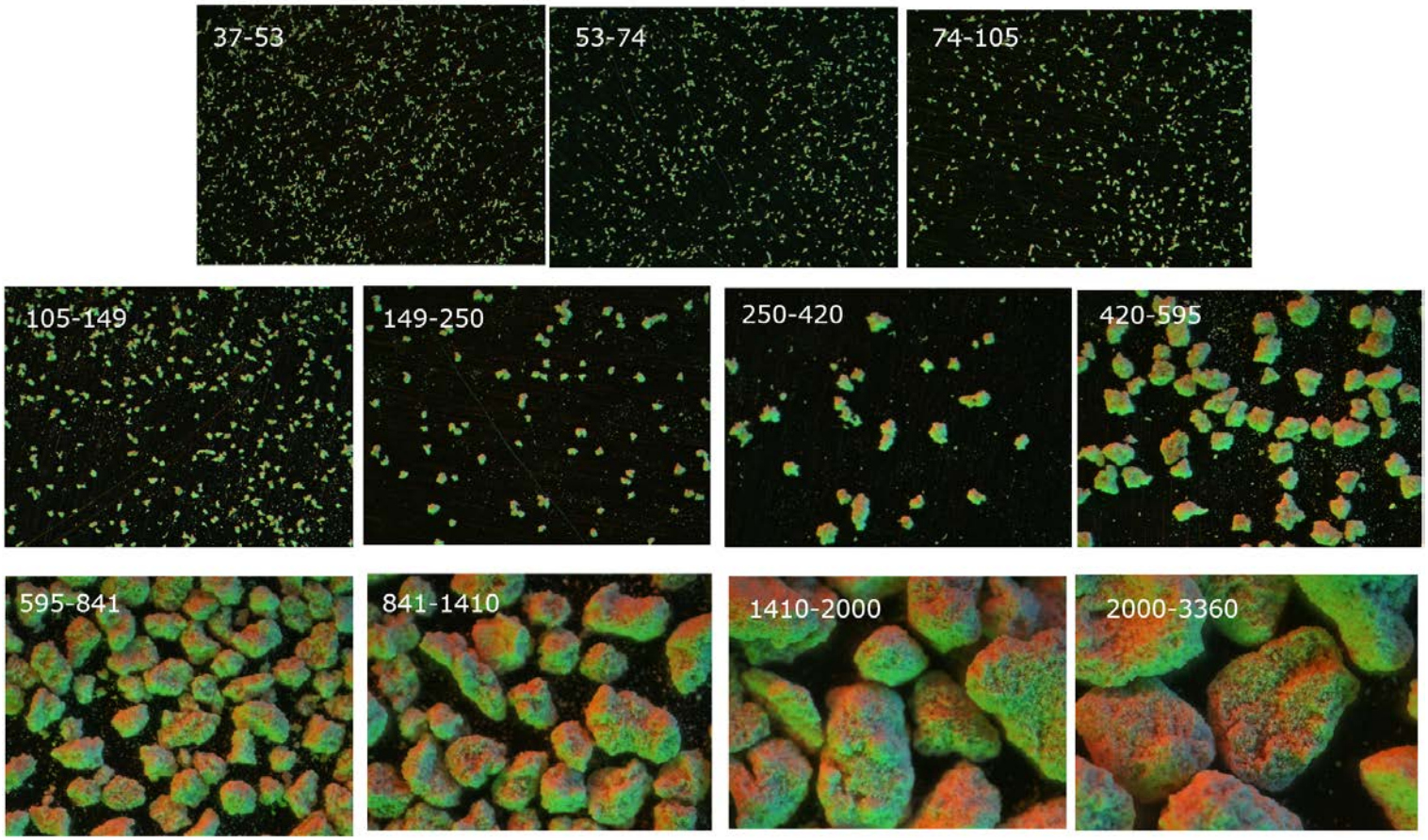

Fig. 2-21 Granules under different size ranges

Chapter 3

From Blends to Tablets: Influence of Formulation and Process Parameters

3.1 Objectives

During pharmaceutical manufacturing, the properties of blends and tablets are sensitive to formulation and process changes. The characteristic properties of blends are bulk density and cohesion representing both static and dynamic behavior. The tensile strength is an important attribute of tablet quality. An investigation of formulation and process parameters on these indexes can provide better understanding for product development and process optimization.

In this chapter, a DoE approach was used to characterize the effects of formulation and process variation on pharmaceutical blends and tablet properties. Also, the correlation between blend properties and tablet properties was determined, which will provide a Quality by Design approach especially in a continuous manufacturing scenario.

3.2 Materials and Methods

Table 3-1. Pharmaceutical Powders with corresponding particle size

Material	Mean(μm)	d10(μm)	d50(μm)	d90(μm)	Vendor
Semifine Acetaminophen	48.93	5.55	32.62	122.7	Mallinckrodt
Avicel PH102	140.0	34.0	121.0	244.1	FMC biopolymer
Fast-Flow Lactose	113.5	54.3	113.3	173.6	Foremost Farms
Regular Lactose	71.88	10.29	63.48	157.7	Foremost Farms

Table 3-1 shows the particle size distribution and properties of materials used in the experiments. A fractional factorial design is used here. The flow behavior of granular

materials and tablet tensile strength are investigated as two responses. The methods used for powder flow characterization include the measurement of Bulk Density and Cohesion. Three formulation factors and one process factor are controlled at two levels, i.e., API Concentration (9% and 45%), Avicel Ratio (0% and 5%) and Lactose Type (Fastflow and Regular) and Lubrication Level (30s and 90s), as shown in Table 3-2. They are labeled as “A”, “B”, “C” and “D” respectively for covenience. The results were analyzed by Minitab.

Table 3-2. Values for the low(-1) and high(+1) levels of input variables investigated in the factorial design

	Input Variable	Low(-1)	High(+1)
A	APAP Concentration	9%	45%
B	Avicel PH102 Ratio	0%	5%
C	Lactose Type	Fast flow	Regular
D	Lubrication Level	30s	90s

In Table 3-3, it shows the runs of experiments and the corresponding responses, namely cohesion, tensile strength and bulk density. In terms of the manufacturing process, powders were first sieved to remove aggomerates and ensure the blend uniformity. After weighing the powders according to the designed formulation, Acetaminophen and Avicel PH102, together with the lubricant MgSt, were mixed in the LabRAM. The lubricant was added separately to avoid overlubrication. Finally, the flow properties and density of blends were measured in FT4 powder rhometer and tablets were manufactured in Fette P2100 36 stations. The hardness was measured in Dr. Schleuniger Model 6D tablet tester. Breaking force can be converted into tensile strength by the following equation

$$\sigma_t = \frac{2F}{\pi dh} \qquad 3\text{-}1$$

σ_t is the tablet tensile strength (MPa), F is the tablet break force (N), d and h is the tablet diameter and thickness, respectively.

Table 3-3 Design of experiments followed by a 2^(4-1) fractional factorial design with two replicates

		Coded Factors										
StdOrder	Run Order	A	B	C	D	Run Label	Cohesion(kPa)		Tensile Strength(N/m^2)		Bulk Density(g/ml)	
6	1	1	-1	1	-1	ac	0.802	0.846	54.829	53.799	0.665	0.646
2	2	1	1	1	1	abcd	1.089	0.923	22.338	23.319	0.742	0.725
4	3	1	-1	-1	1	ad	1.315	1.35	54.808	53.274	0.615	0.625
5	4	-1	1	1	-1	bc	0.122	0.11	39.41	36.982	0.71	0.705
8	5	-1	1	-1	1	bd	0.444	0.439	113.325	108.957	0.705	0.705
3	6	-1	-1	-1	-1	-1	0.746	0.896	48.532	42.608	0.781	1.143
1	7	-1	-1	1	1	cd	1.234	1.203	147.696	148.887	0.751	1.072
7	8	1	1	-1	-1	ab	0.163	0.247	43.464	48.532	0.662	0.976

3.3 Results and Discussion

3.3.1 Cohesion

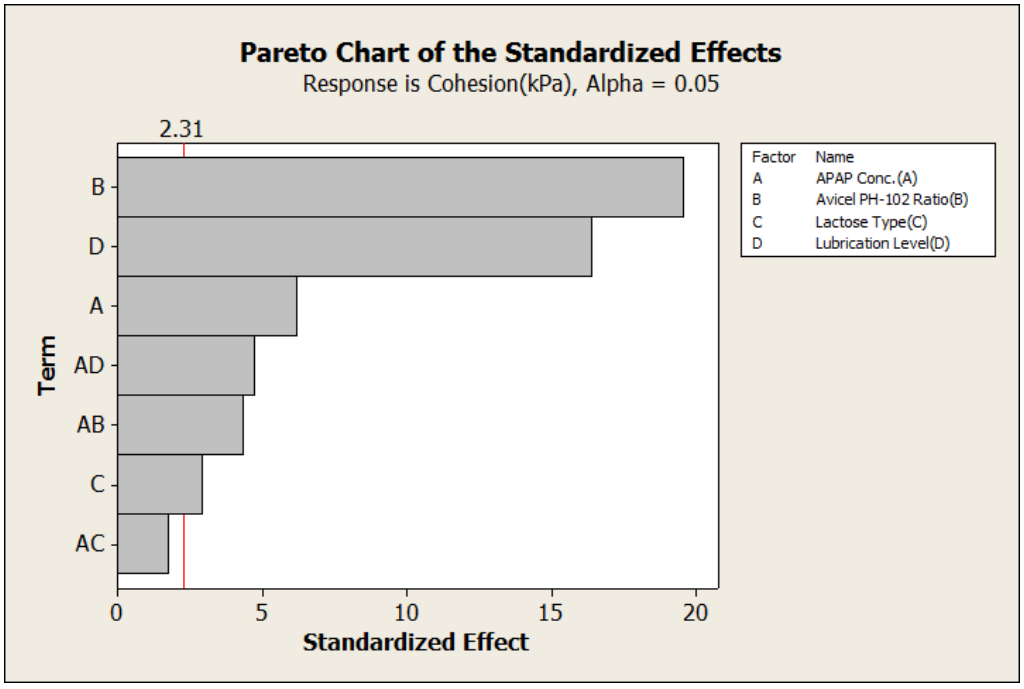

Fig. 3-1 Pareto Chart of the standardized effects for cohesion

According to Fig. 3-1, all the main effects including process parameters and formulation parameters significantly influence the cohesion. Besides, there are two interaction effects, AB and AD, that are also statistically significant. In Fig. 3-2, it indicates how the main effects influencing the cohesion. Basically, cohesion increases with the increase of API concentration and lubrication time. It also slightly increases when the regular lactose replaces fast flow lactose as regular lactose is more cohesive that fast flow lactose. With longer lubrication time, more energy was applied to the blends, thus improving the flowability. Since Avicel PH102 flows better than API, a larger proportion of Avicel PH102 significantly decreases the cohesion.

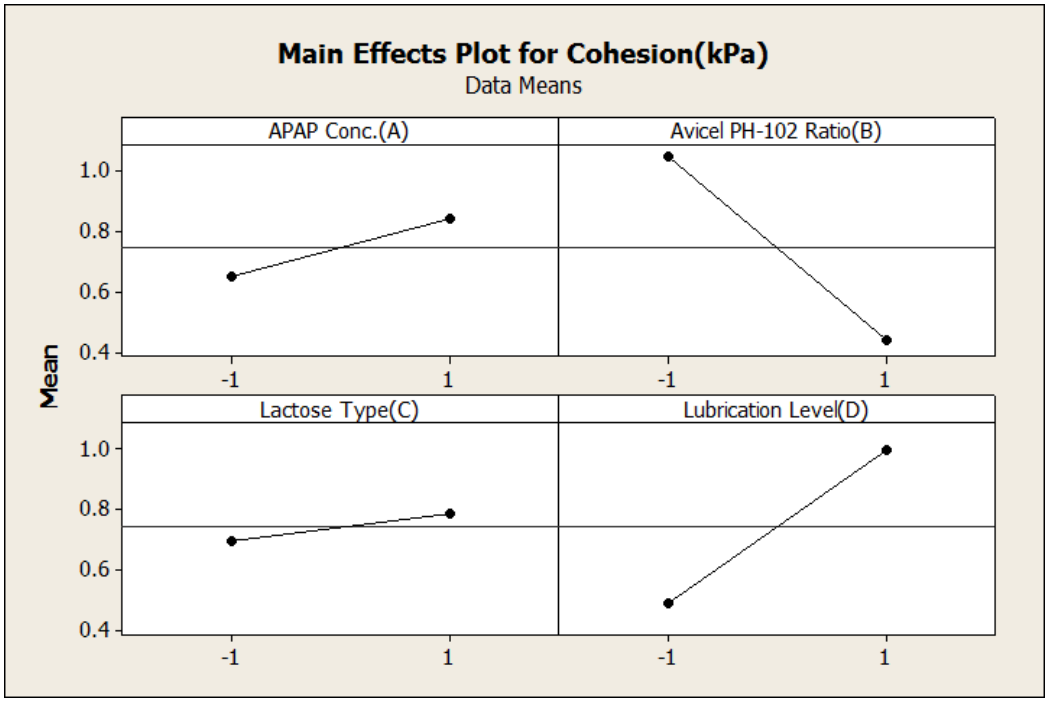

Fig. 3-2 Main Effects Plot for cohesion

Fig 3-3 illustrates how the effects interact with each other. With the lower level of API concentration, cohesion decreases more significantly with the increase of Acivel PH102 and increases less significantly by increasing the lubrication time. To achieve the lowest

cohesion, the combination of low level of API concentration and lubrication time, fast flow lactose and high level of Avicel PH102 is desired. However, as shown in Fig. 3-4 (question mark), the results of this combination are not available because of the fractional factorial design. A prediction model should be built and used to predict the unavailable results.

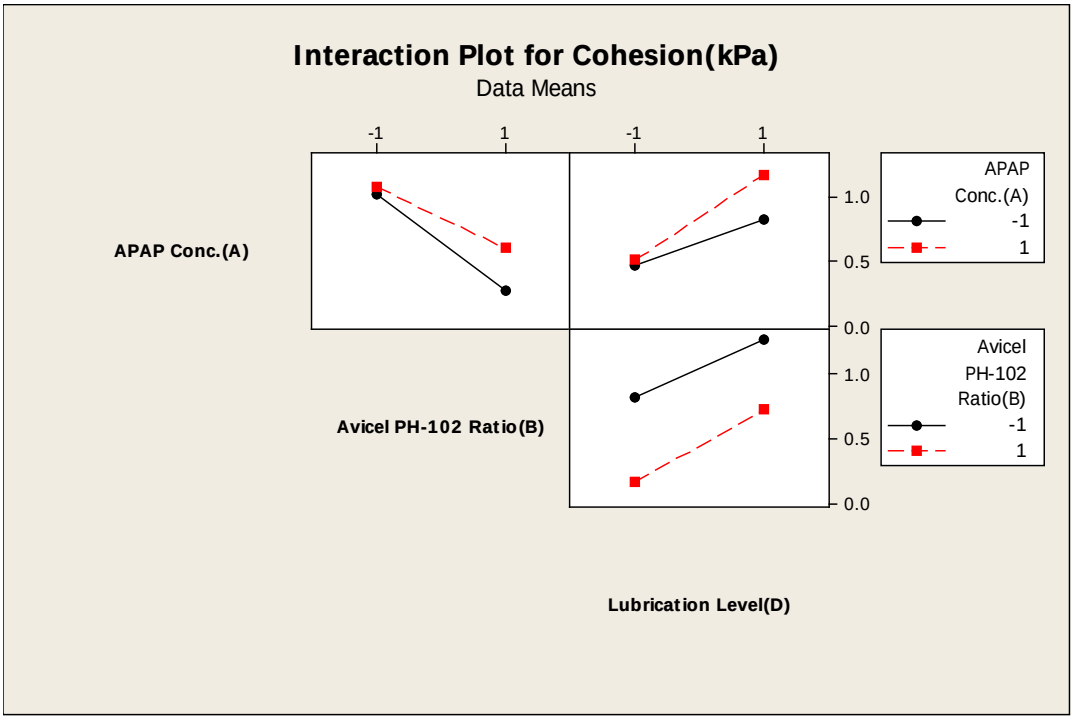

Fig. 3-3 Interaction Plot for cohesion

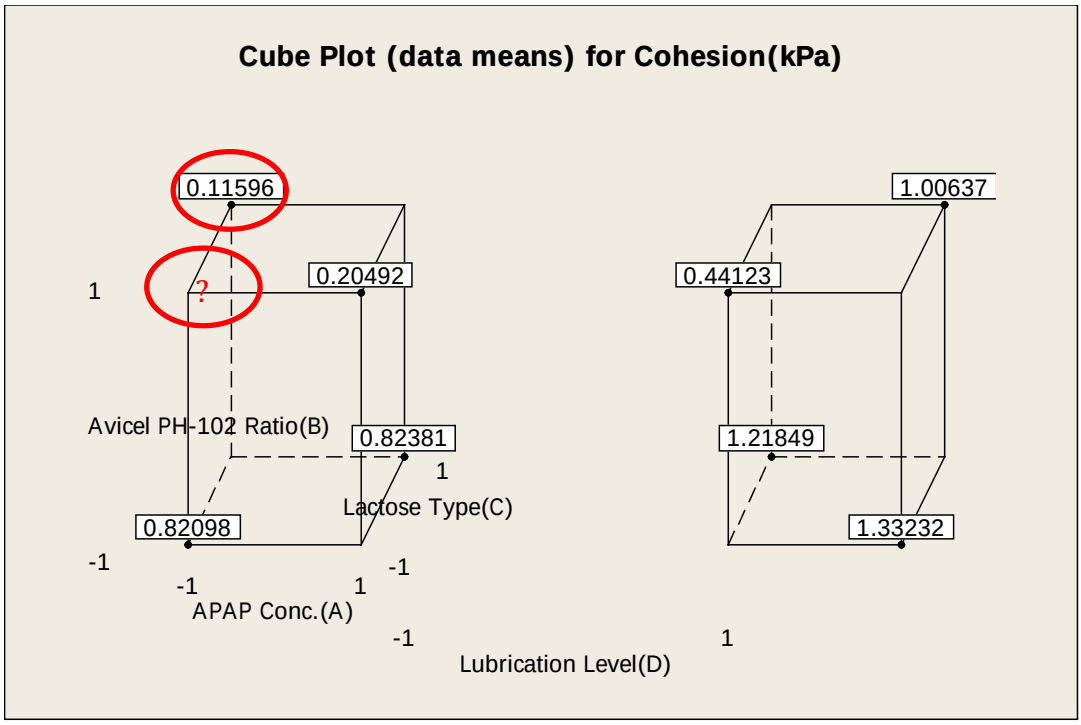

Fig. 3-4 Cube Plot for cohesion

The software, Minitab, generates the optimization plot as shown in Fig. 3-5. Assuming the first order model is adequate for describing the relation between cohesion and factors, the model is

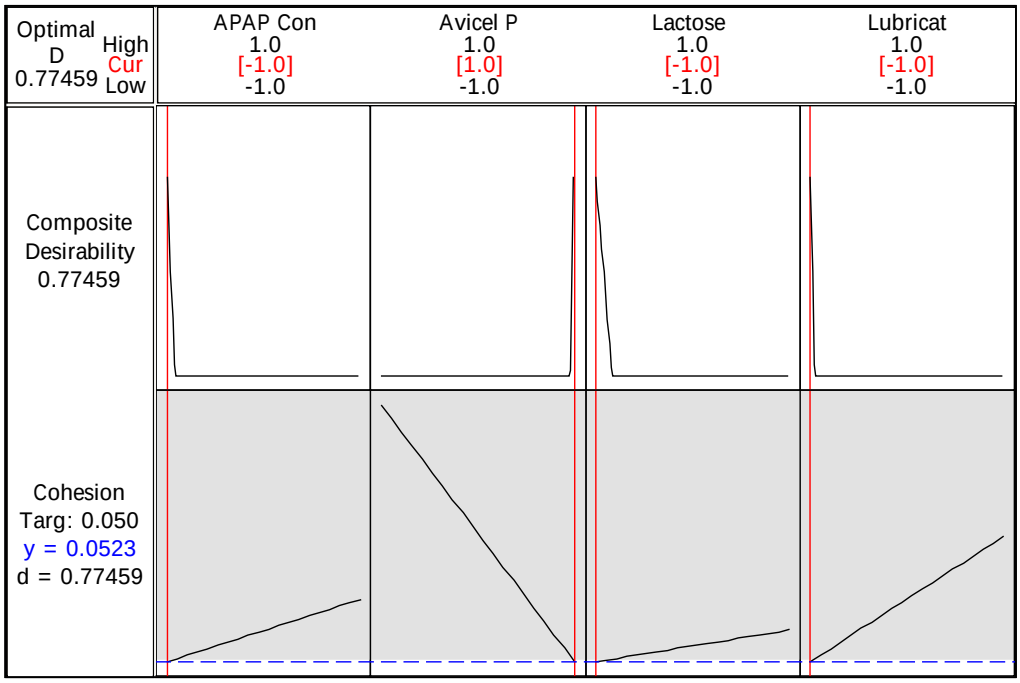

Fig. 3-5 Optimization Plot for cohesion

$$Y = 0.7455 + 0.0963X_A - 0.3034X_B + 0.0456X_C + 0.2541X_D + 0.0672X_{AB} + 0.0734X_{AD} \quad 3\text{-}2$$

By simulating with above model, the lowest achievable cohesion is 0.0523. Since the desirability evaluates how a combination of operation parameters satisfies the desired response, a desirability of 0.7746 indicates that it is not quite effective at minimizing the cohesion. One Also, based on the limited data set, residuals did not appear to be problematic.

3.3.2 Bulk Density

Before reducing the order of model, as shown in Fig. 3-6, the only factor that can significantly influence the bulk density is the interaction effect of API concentration (A) and Avicel PH-102 ratio (B). And the R-square is only 16.62%, which illustrates that results were quite unreliable. From Fig. 3-7, there is a significant difference between originals and replicates. Therefore, blocking was considered here as an effective approach to smooth out the difference.

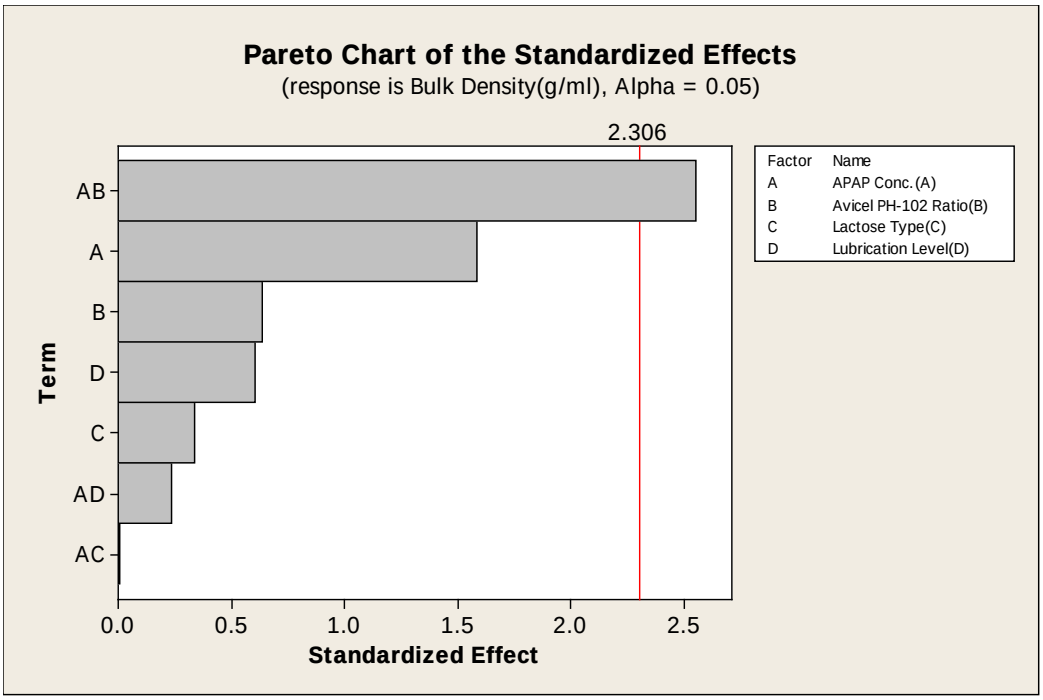

Fig. 3-6 Pareto Chart of the standardized effects for bulk density

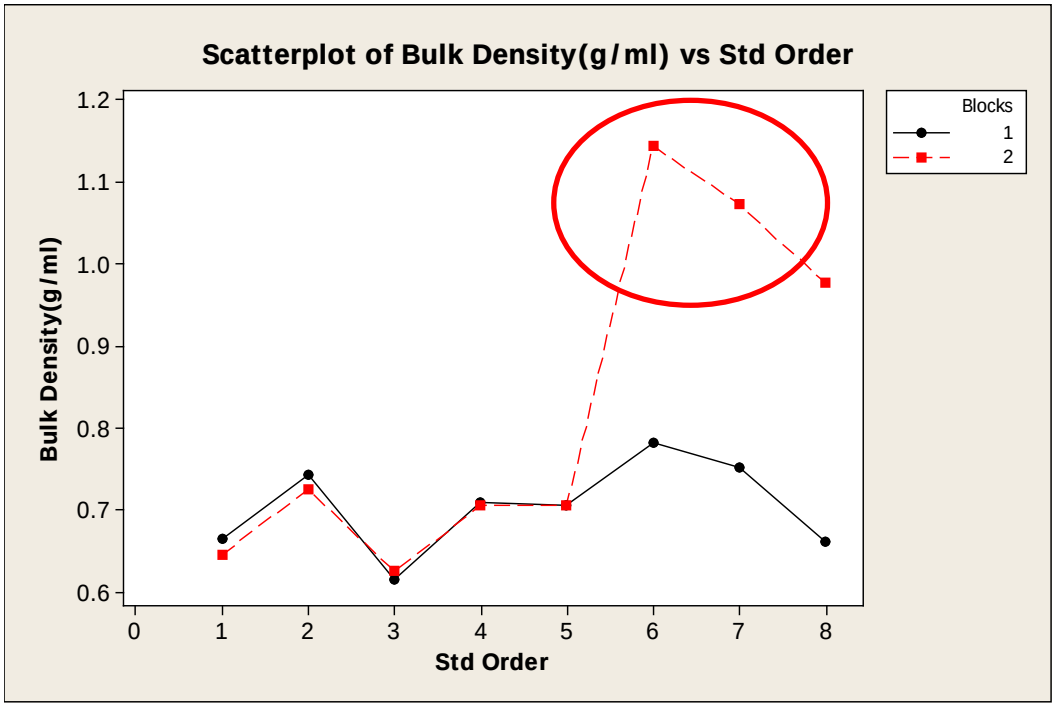

Fig. 3-7 Scatterplot of bulk density versus experimental order

Fig. 3-8 shows the Pareto Chart after blocking the orginal experiments and replicates and reducing the model order. The R-square now increases up to 56.52% and significant

effects include interaction effect of API concentration (A) and Avicel PH-102 ratio (B) as well as the main effect of API concentration.

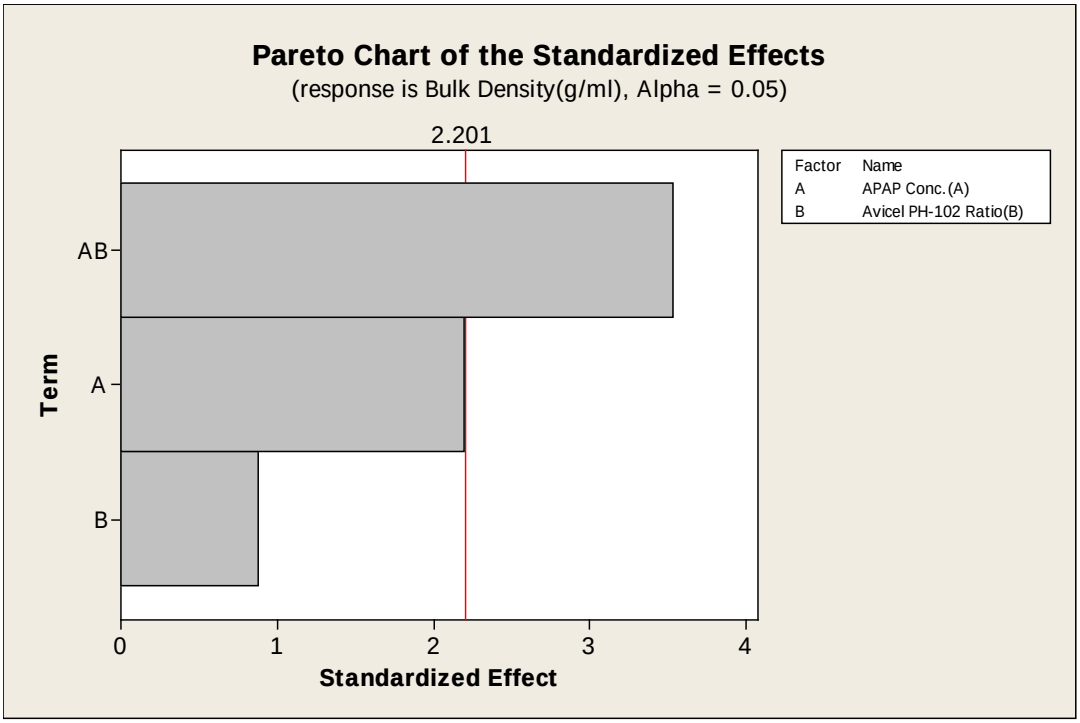

Fig. 3-8 Pareto Chart for bulk density after blocking and reducing model order

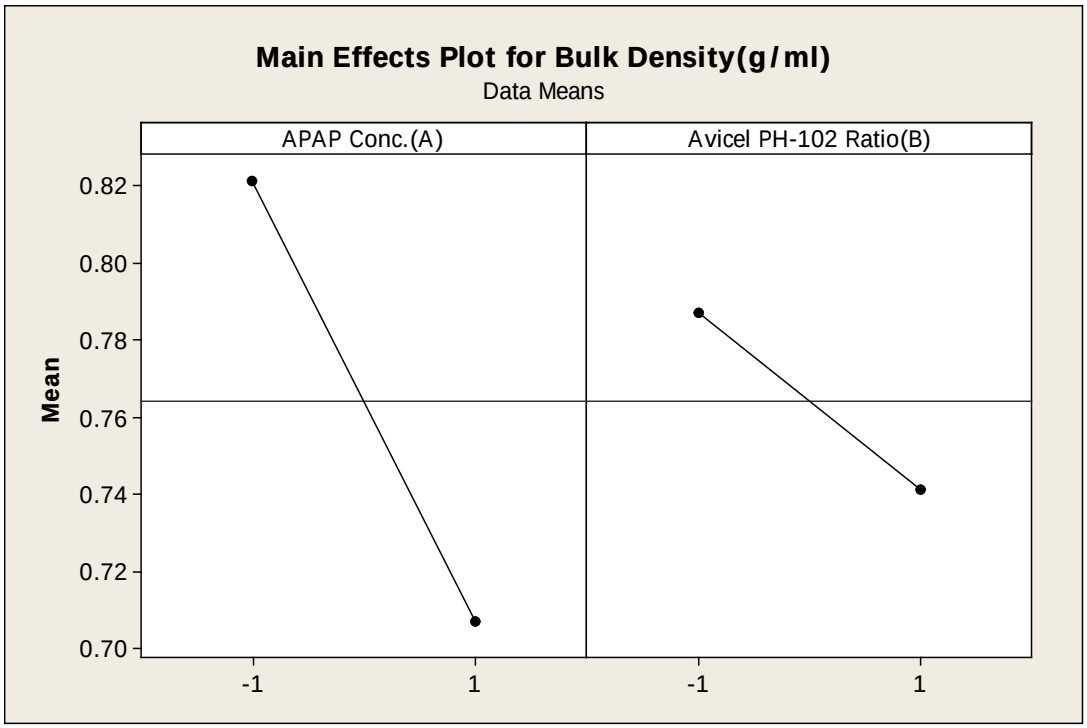

Fig. 3-9 Main Effects Plot for Bulk Density

Fig. 3-9 and 3-10 illustrate the main effects plot and interaction effect plot. High API concentration reduces bulk density. There exists strong interaction effect, namely that at high API concentration, bulk density increases as the Avicel PH102 increases. However, at low level of API concentration, bulk density decreases the Avicel PH102 proportion increases.

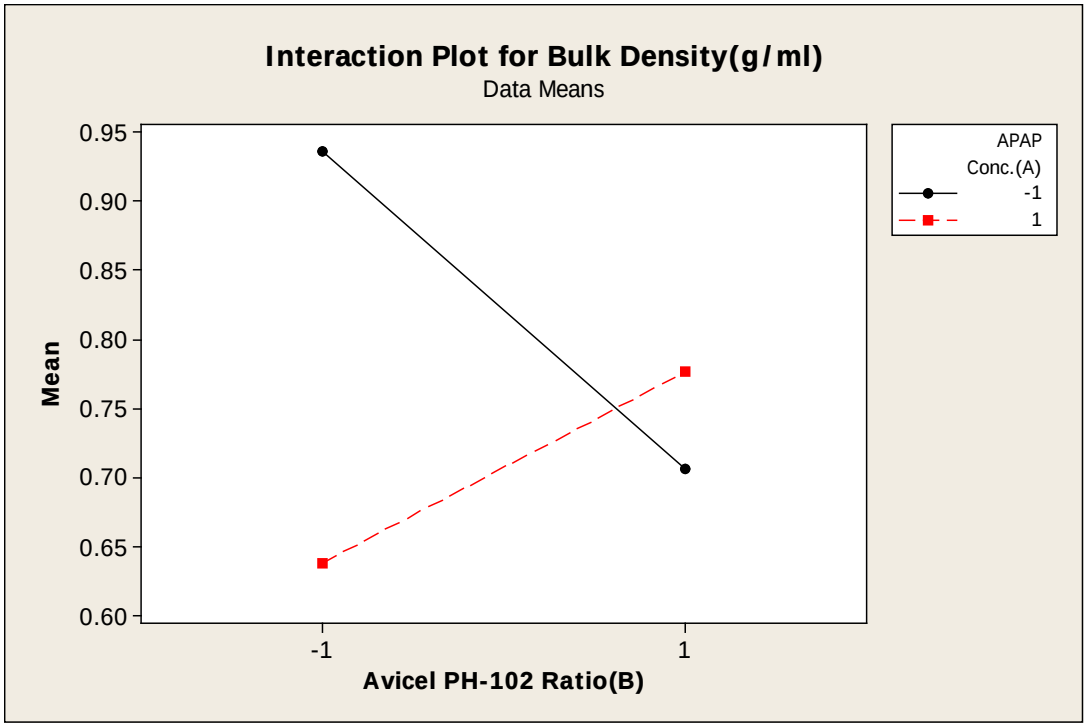

Fig. 3-10 Interaction Plot for Bulk Density

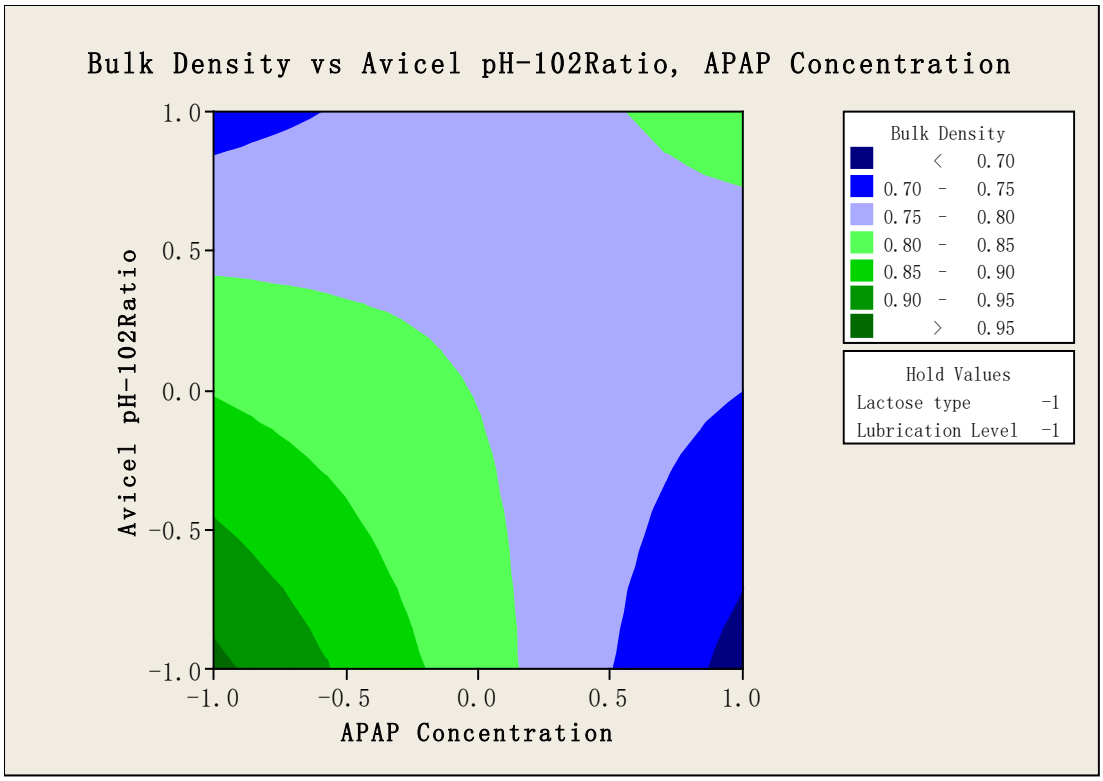

Fig. 3-11 Contour Plot for Bulk Density

Finally, Fig. 3-11 shows the contour plot for bulk density while holding the two factors of lactose type and lubricant level at fast flow lactose and 30 seconds respectively. It is in accordance with the previous analysis, i.e., a low level of API concentration and excipient can give rise to the highest bulk density.

3.3.3 Tensile Strength

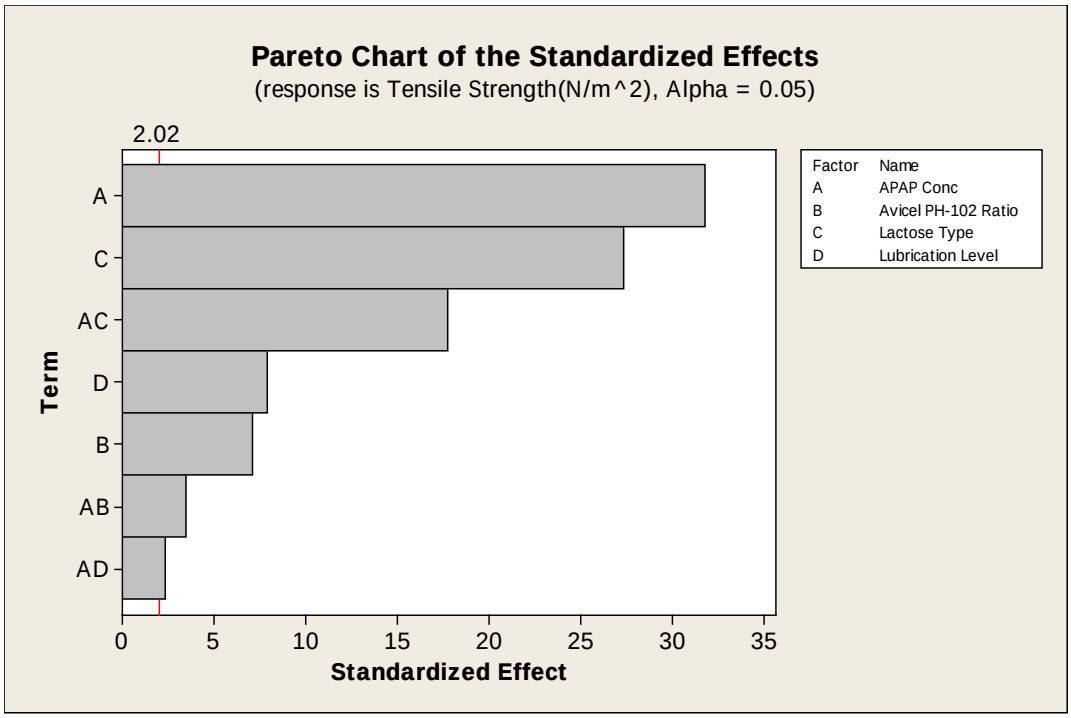

Fig. 3-12 Pareto Chart of the standardized effects for tensile strength

For the tensile strength, all main effects are statistically significant. The interaction effects of APAP concentration with all the remaining factors are also significant. It indicates that tensile strength is sensitive to both process parameters and formulation. Fig. 3-13 and Fig. 3-14 show the main effects and interaction effects on the tensile strength. The tensile strength can be enhanced by increasing the concentration of Avicel PH102 or adding regular lactose. In contrast, it is adversely propertional to API concentration and lubrication time. There are mild interaction effects that exist between the API concentration and other parameters. Specifically, high APAP concentration reduces the effects of Avicel PH 102 and lactose type and lubrication time. Without reducing the model order, the R-square approaches 97.9%, which demonstrates the reliability of analysis results. From the cube plot, Fig. 3-15, it illustrates that a highest tensile strength

is achievable at low level of lubrication time and APAP concentration, high level of Avicel PH102 and regular lactose.

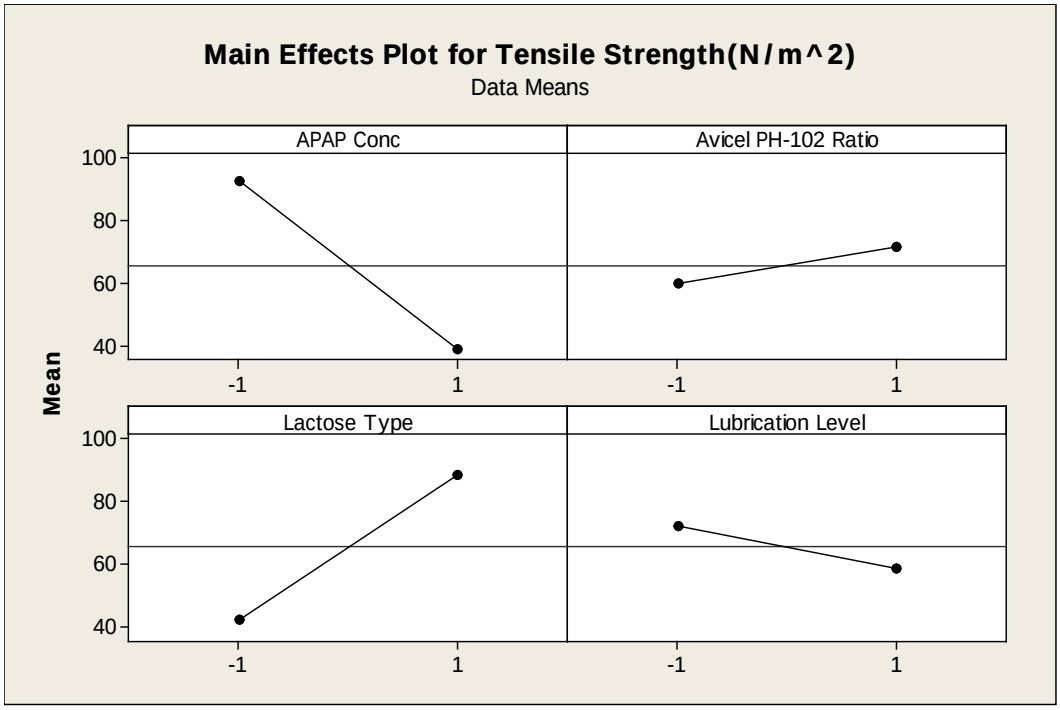

Fig. 3-13 Main Effects Plot for Tensile Strength

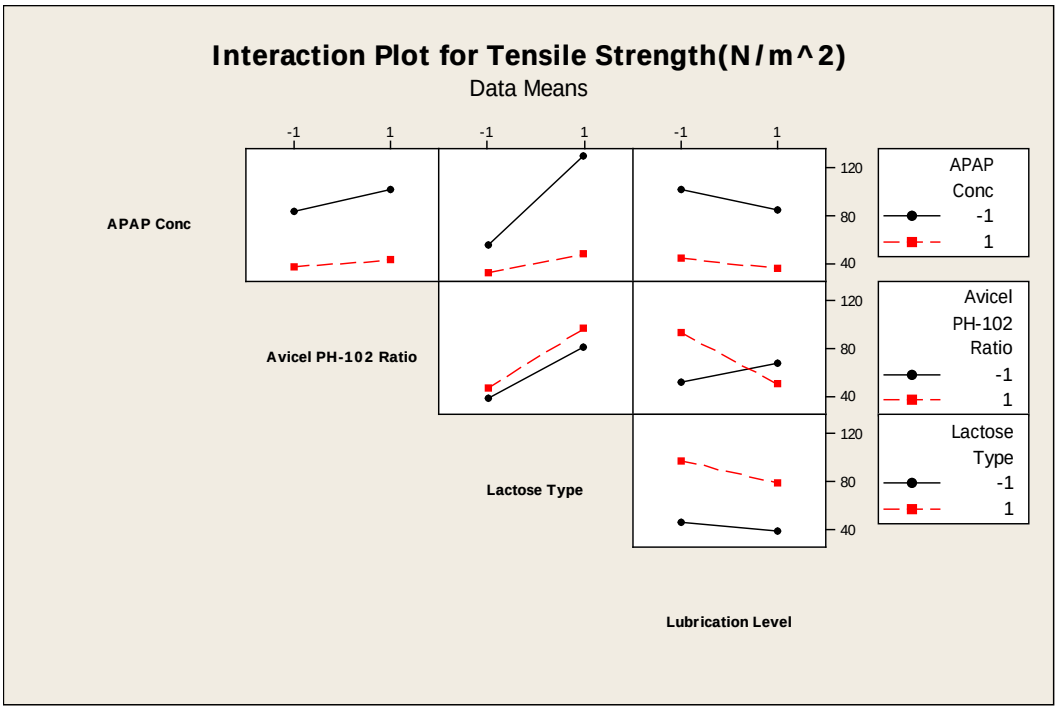

Fig. 3-14 Interaction Effects Plot for Tensile Strength

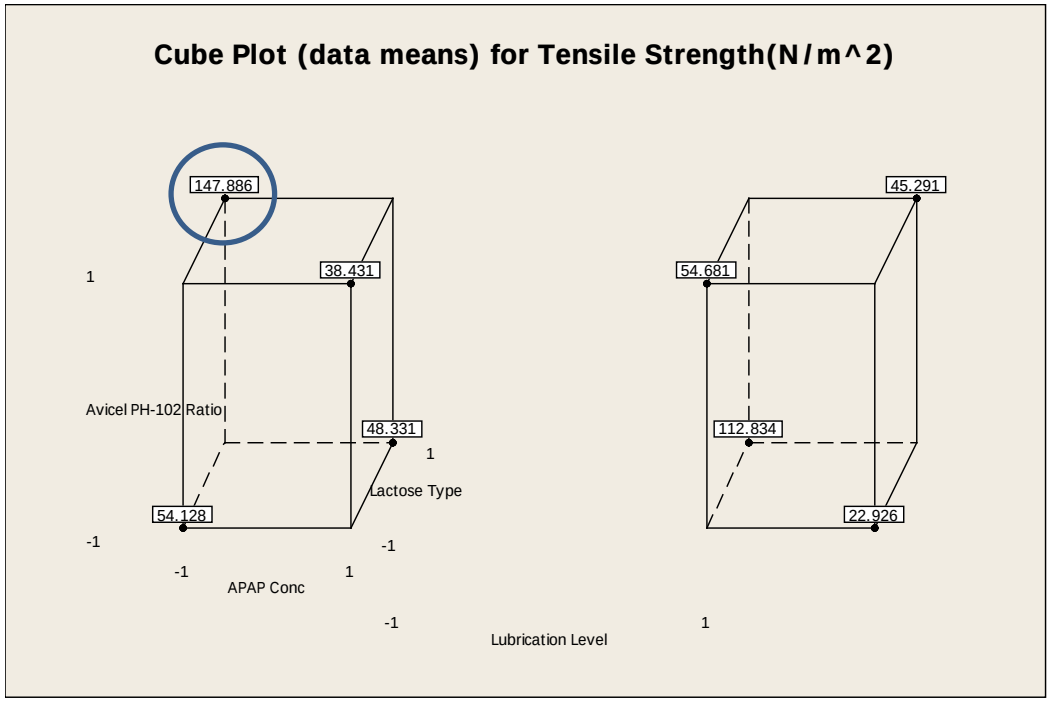

Fig. 3-15 Cube Plot for tensile strength

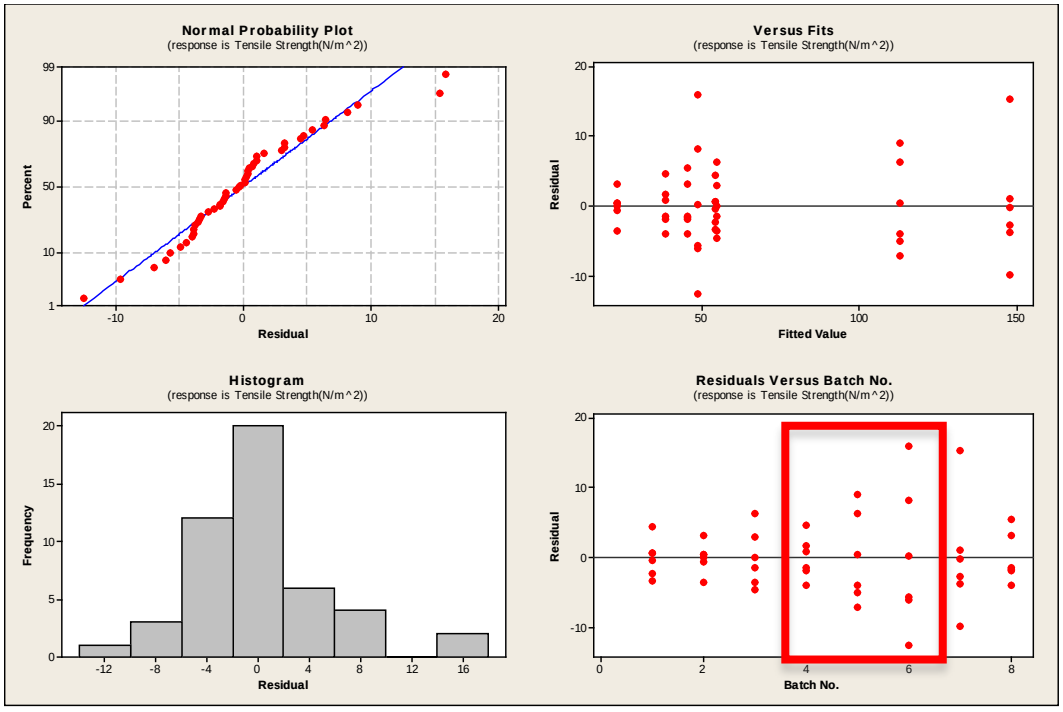

Fig. 3-16 Residuals Plots for tensile strength

Also, a first order model was built to predict the tensile strength, which is in agreement with the experimental results.

$$Y = 65.56 - 26.82 * X_A + 6.01 * X_B + 23.02 * X_C - 6.63 * X_D - 2.89 * X_{AB} - 14.96 * X_{AC} + 1.99 * X_{AD}$$

3-3

Fig. 3-16 shows the residuals plots tensile strength. The histogram and normal probability plot displays that residuals are normally distributed. The fitted plot displays that residual values are independent of Tensile Strength magnitude and residuals are fairly high. The residuals appears to large in batch 5, 6 and 7.

3.3.4 Correlation

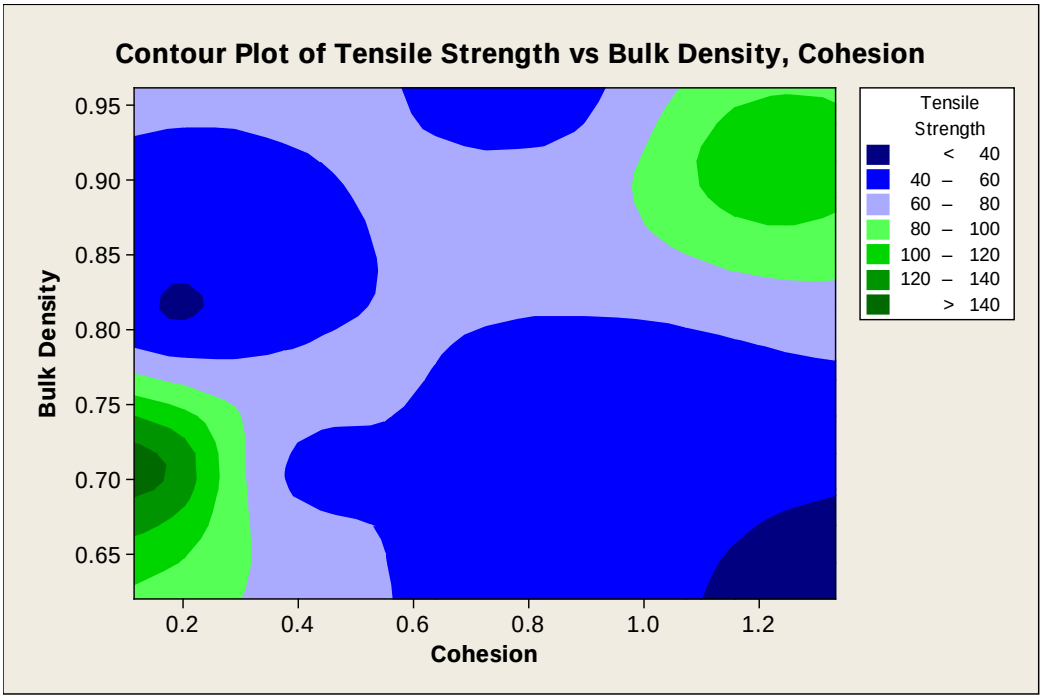

Fig. 3-17 Contour Plot between tensile strength, bulk density and cohesion

The properties of tablets are related to powder density and flowability. The map in Fig. 3-17 shows that tensile strength is highest at a low bulk density and cohesion or high bulk density and cohesion. In contrast, it becomes relatively low when bulk density is high and

cohesion is low and vice versa. It seems that the interaction effect between cohesion and bulk density can significantly influence the tensile strength. However, it is difficult to find a quantitative relationship between tensile strength and bulk density and cohesion. According to the experimental conditions, it is more scientifically sound to predict tablet tensile strength based on excipient and API content as suppose to the bulk density and cohesion properties.

3.4 Summary

From blends to tablets, the levels of excipient, API content, and lubricant had a significant and usable effect on cohesion and tensile strength. Bulk density appear to be fair less dependent on our factors. Tensile strength prediction based on Excipient, API content, and Lubricant levels has higher utility than prediction based on powder properties.

Chapter 4

Conclusions and future prospectives

4.1 Conclusion

In this dissertation, a continuous high-shear wet granulator was characterized based on a placebo formulation comprising of 70% ∂-lactose monohydrate and 30% microcrystalline cellulose. An I-optimal design of experiments was conducted to investigate the influence of several crucial variables on granule properties. These include two process parameters, rotation speed and L/S ratio and two design parameters, blade configuration and nozzle position. Rotation speed and L/S ratio were found to be the most important factors in determining the granules properties.

For this Glatt continuous granulator, an optimum operational condition for this lactose and MCC formulation was L/S ratio 0.3 and rotation speed at approximately 275RPM or 660RPM. These operation conditions provide the maximum hold up and energy input, thus producing a more desirable particle size distribution. The largest D50 is around 200 microns while the largest growth ratio is about 2. Granules from all selected batches are either easy-flowing or free flowing. The compaction highly depends on the granules particle size distribution after milling. Overall, it decreases with the increase of D50. The granules compactability from batch 4 and 14 are close to each other because of the same L/S ratio. Since granules of batch 14 are fluidized and densified, it produced granules with smaller porosity and was relatively less compressible than batch 4.

4.2 Suggestion for future work

In this thesis, the focus was on the parametric analysis of Glatt high shear continuous granulator. Based on the penetration test, improved granulation performance would be achievable if the dripping mode nozzle was replaced by spraying mode nozzle. In general, a relatively small droplet size is conducive to accelerating the penetration process. Also, porosity is an important attribute of granules, which could be tested by mercury intrusion porosimetry. This is important because it is directly related to the tablet hardness. To have a better understanding of the powder flow behavior inside the granulator, residence time distribution test is highly recommended. Given different granulation mechanisms, it would be meaningful to compare the performance of this Glatt granulator to other granulators, such as the Lodige continuous high shear granulator, twin screw granulator (Thermo Pharma 16 TSG) and batch high shear granulator (Diosna P 1-6).

Reference

[1] Litster, J.D., Ennis, B.J., The Science and Engineering of Granulation Process, Kluwer Academic Publishers, Dordrecht, The Netherlands, 2004.

[2] Kristensen, H.G., Schaefer, T. Granulation - a review of pharmaceutical wet-granulation. Drug Dev Ind Pharm 13 (1987) 803-872.

[3] Rumpf, H. Grundlagen und Methoden des Granulierens. Chem Ing Tech 3 (1958) 144-158.

[4] Guerin, E., Tchoreloff, P., Leclerc, B., Tanguy, D., Deleuil, M., Couarraze, G., Rheological characterization of pharmaceutical powders using tap testing, shear cell and mercury porosimeter. Int J Pharm 189 (1) (1999) 91-103.

[5] Gabaude, C.M.D., Gautier, J.C., Saudemon, P. Validation of a new pertinent packing coefficient to estimate flow properties of pharmaceutical powders at a very early development stage, by comparison with mercury intrusion and classical flowability methods. J Mater Sci 36 (7) (2001) 1763-1773.

[6] Faure, A., York, P., Rowe, R.C. Process control and scale-up of pharmaceutical wet granulation processes: a review. Eur J Pharm Biopharm 52 (3) (2001) 269-277.

[7] Augsburger, L.L., Vuppala, M.K. Theory of granulation. In: Parikh, D.M. (Ed.). Handbook of pharmaceutical granulation technology. Marcel Dekker: New York (1997) 7-25.

[8] Miller, R. W. and D. M. Parikh. Chapter 6: Roller Compaction Technology. Handbook of pharmaceutical granulation technology Taylor & Francis, 2005.

[9] Freitag, F. and P. Kleinebudde. "How do roll compaction/dry granulation affect the tableting behaviour of inorganic materials? Comparison of four magnesium carbonates." Eur J of Pharm Sci 19 (4) (2003) 281-289.

[10] Holm P., Jungersen O., Schaefer T., Kristensen H.G. Granulation in high-speed mixers. 1. Effect of process variables during kneading. Pharm Ind 45 (1983) 806-811.

[11] Rubino O. R. Fluid-bed technology: overview and criteria for process selection. Pharm Tech 6 (1999) 104-113.

[12] Vervaet, C., Baert, L., Remon, J.P. Extrusion-spheronisation A literature review. Int J Pharm 116 (2) (1995) 131-146.

[13] Banks M., Aulton M. E. Fluidised bed granulation: a chronology. Drug Dev Ind Pharm 17 (1991) 1437-1463.

[14] Bonde M. Continuous granulation. In: Parikh, D.M. (Ed.). Handbook of pharmaceutical granulation technology. Marcel Dekker: New York (1997) 368-387.

[15] Keleb E. I., Vermeire A., Vervaet C., Remon J. P. Twin screw granulation as simple and efficient tool for continuous wet granulation. Int J Pharm 273 (1) (2004) 183-194.

[16] Hapgood, K.P., Litster, J.D., Smith, R. Nucleation regime map for liquid bound granules. AIChE J 49 (2) (2003) 350-361.

[17] Hapgood, K.P., Litster, J.D., Biggs, S.R., Howes, T. Drop penetration into porous powder beds. J Colloid Interface Sci 253 (2) (2002) 353-366.

[18] Litster, J.D., Hapgood, K.P., Michaels, J.N., Sims, A., Robert, M., Kameneni, S.K., Hsu, T. Liquid distribution in wet granulation: dimensionless spray flux. Powder Tech 114 (1) (2001) 32-39.

[19] Iveson, S.M., Litster, J.D. Growth regime map for liquid bound granules. AIChE J 44 (7) (1998) 1510-1518.

[20] Tardos, G.I., Khan, M.I., Mort, P.R. Critical parameters and limiting conditions in binder granulation of fine powders. Powder Tech 94 (3) (1997) 245-258.

[21] Iveson, S.M., Wauters, P.A.L., Forrest, S., Litster, J.D., Meesters, G.M.H., Scarlett, B. Growth regime map for liquid-bound granules: further development and experimental validation. Powder Tech 117 (1) (2001) 83-97.

[22] Liu, L.X., Litster, J.D., Iveson, S.M., Ennis, B.J., Coalescence of deformable granules in wet granulation processes. AIChE J 46 (3) (2000) 529-539.

[23] Iveson, S.M., Litster, J.D., Hapgood, K., Ennis, B.J. Nucleation, growth and breakage phenomena in agitated wet granulation processes: a review. Powder Tech 117 (1) (2001) 3-39.

[24] Liu, L.X., Smith, R., Litster, J.D. Wet granule breakage in a breakage only high shear mixer: effect of formulation properties on breakage behaviour. Powder Tech 189 (2) (2009) 158-164.

[25] CFR-Code of Federal Regulations. Title 21, Volume 4, Part 210, 2014.

[26] Leuenberger, H. New trends in the production of pharmaceutical granules: batch versus continuous processing. Eur J Pharm Biopharm 52 (3) (2001) 289 - 296.

[27] Vervaet, C., Remon, J.P. Continuous granulation in the pharmaceutical industry. Chem Eng Sci 60 (14) (2005) 3949 - 3957.

[28] Lindberg,N.O. Some experience of continuous granulation. Acta Pharm Suec 25 (1988) 239 - 246.

[29] Food and Drug Adminitration CDER, Guidance for Industry Q8 Pharmaceutical Development, May 2006.

[30] Food and Drug Administration CDER, Guidance for Industry Q8(R2) Pharmaceutical Development, November 2009.

[31] M. Nasr, Quality by Design (QbD) opportunities, challenges and future direction, In: AIChE Annual Meeting, Minneapolis, 2011.

[32] P.C. Collins, QbD - it's not just for breakfast anymore, In: AIChE Annual Meeting, Minneapolis, 2011.

[33] Guidance for Industry PAT - A Framework for Innovative Pharmaceutical Development, Manufacturing, and Quality Assurance, FDA, 2004.

[34] Hemati M., Cherif R., Saleh K., Pont V. Fluidized bed coating and granulation: influence of process-related variables and physicochemical properties on the growth kinetics. Powder Tech 130 (1) (2003) 18-34.

[35] Tan H.S., Salman A.D., Hounslow M.J., Kinetics of fluidised bed melt granulation V: simultaneous modelling of aggregation and breakage. Chem Eng Sci 60 (14) (2005) 3847-3866.

[36] Tan H.S., Salman A.D., Hounslow M.J., Kinetics of fluidised bed melt granulation III: tracer studies. Chem Eng Sci 60 (14) (2005) 3835-3845.

[37] Tan H.S., Salman A.D., Hounslow M.J., Kinetics of fluidised bed melt granulation I: the effect of process variables. Chem Eng Sci 61 (5) (2006) 1585-1601.

[38] Gamlen M. J., Eardley C. Continuous extrusion using a Baker Perkins MP50 (multipurpose) extruder. Drug Dev Ind Pharm 12 (1986) 1701-1713.

[39] Lindberg N. O., Tufvesson C., Olber L. Extrusion of an effervescent granulation with a twin screw extruder, Baker Perkins MPF 50 D. Drug Dev Ind Pharm 13 (1987) 1891-1913.

[40] Keleb E.I., Vermeire A., Vervaet C., Remon J.P. Continuous twin screw extrusion for the wet granulation of lactose. Int J Pharm 239 (1) (2002) 69-80.

[41] Djuric D., Kleinebudde P. Continuous granulation with a twin-screw extruder: Impact of material throughput. Pharm Dev Tech 15 (5) (2010) 518-525.

[42] EI Hagrasy A.S., Hennenkamp J.R., Burke M.D., Cartwright J.J., Litster J.D. Twin screw wet granulation: Influence of formulation parameters on granule properties and growth behavior. Powder Tech 238 (2013) 108-115.

[43] Djuric D., Kleinebudde P. Impact of screw elements on continuous granulation with a twin-screw extruder. J Pharm Sci 97 (11) (2008) 4934-4942.

[44] Thompson M.R., Sun J. Wet granulation in a twin-screw extruder: implication of screw design. J Pharm Sci 99 (4) (2009) 2090-2103.

[45] Dhenge R.M., Fyles R.S., Cartwright J.J., Doughty D.G., Hounslow M.J., Salman A.D. Twin screw wet granulation: Granule properties. Chem Eng J 164 (2) (2010) 322-329.

[46] Vercruysse J., Cordoba Diza D., Peeters E., Fonteyne M., Delaet U., Van Assche I., De Beer T., Remon J.P., Vervaet C. Continuous twin-screw granulation: Influence of process variables on granule and tablet quality. Eur J Pharm Biopharm 82 (1) (2012) 205-211.

[47] Lee K.T., Ingram A., Rowson N.A. Comparison of granule properties produced using Twin Screw Extruder and High Shear Mixer: A step towards understanding the mechanism of twin screw wet granulation. Powder Tech 238 (2013) 91-98.

[48] Kayrak-Talay D., Litster J.D. A priori performance prediction in pharmaceutical wet granulation: Testing the applicability of the nucleation regime map to a formulation with a broad size distribution and dry binder addition. Int J Pharm 418 (2) (2011) 254-264.

[49] Kayrak-Talay D., Dale S., Wassgren C., Litster J.D. Quality by design for wet granulation in pharmaceutical processing: Assessing models for a priori design and scaling. Powder Tech 240 (2013) 7-18.

[50] Vanarase A.U., Muzzio F.J. Effect of operating conditions and design parameters in a continuous powder mixer. Powder Tech 208 (2011) 26-36.

[51] Pandey P., Tao J., Chaudhury A., Ramachandran R., Gao J.Z., Bindra D.S. A combined experimental and modeling approach to study the effects of high-shear wet granulation process parameters on granule characteristics. Pharm Dev Tech 18 (1) (2013) 210-224.

[52] EI Hagrasy A.S., Cruise P., Jones I., Litster J.D. In-line Size Monitoring of a Twin Screw Granulation Process Using High-Speed Imaging. J Pharm Innov 8 (2) (2013) 90-98.